JOURNAL OF GEOPHYSICAL RESEARCH, VOL. 115, D14118, doi:10.1029/2009JD012883, 2010

Influence of tropical convection on the Southern Hemisphere ozone maximum during the winter to spring transition

M. H. Hitchman[1] and M. J. Rogal[1]

Received 24 July 2009; revised 22 February 2010; accepted 12 March 2010; published 29 July 2010.

[1] During the Southern Hemisphere (SH) winter a zonally asymmetric maximum in column ozone develops south of Australia, which amplifies from August through October. This ozone maximum lies in the band 50–60°S and extends from the southern Indian Ocean to the eastern Pacific. It is proposed that the location of the ozone maximum is due to the geographical distribution of outflow from tropical convection in the upper troposphere and lower stratosphere (UTLS), which is concentrated over the southern Indian Ocean. This southward flow of tropical air creates subtropical anticyclones in the UTLS and provides the angular momentum for the entrance to the Australian westerly jet. The ozone-rich troughs in synoptic waves breaking on the jet contribute to the monthly mean ozone maximum poleward of the jet. As Indonesian convection contracts zonally and shifts eastward during SH spring, so do the Australian jet and ozone maximum. In addition, extratropical planetary waves become more active from August through October. Convective outflow surges lead to amplification of subtropical anticyclones, which often extend into the lower stratosphere and merge with stalling planetary wave ridges. Amplification of these ozone-rich ridges over the high-latitude South Pacific contributes to the eastward shift of the ozone maximum. The UTLS over the southern Indian Ocean appears to be a sensitive region where tropical convection can influence extratropical planetary waves via excitation of subtropical anticyclones and propagation of Rossby wave activity through the connecting westerly waveguide.

Citation: Hitchman, M. H., and M. J. Rogal (2010), Influence of tropical convection on the Southern Hemisphere ozone maximum during the winter to spring transition, *J. Geophys. Res.*, *115*, D14118, doi:10.1029/2009JD012883.

1. Motivation

[2] Monthly mean column ozone in the Southern Hemisphere (SH) winter and spring usually exhibits an elongated ozone maximum (OM) near Australia centered in the band 40–60°S, extending from the southern Indian Ocean (SIO) to the Eastern Pacific (Figure 1). This zonal asymmetry gradually amplifies during winter, reaches its maximum in October, and wanes during November (Figure 1c). As in every spring examined, during 2000 the ozone maximum advanced eastward from ~100°E in August to ~125°E in October (Figure 1). This asymmetry is modulated by eastward-traveling planetary waves, which increase in amplitude during the winter to spring transition, with stalling, amplified ozone-rich ridges contributing to the increased amplitude of the OM (Figure 1c). This fundamental shape has been known for many years [*MacDowall*, 1960; *Godson*, 1963; *London et al.*, 1976], and is often referred to as the "ozone croissant" when seen in polar stereographic projection. Here we focus specifically on the ozone maximum (OM) component of this pattern. The primary goal of this paper is to answer the question: What is the fundamental reason for the geographical location of the OM? Salient features to be addressed include the seasonal intensification and eastward migration of the OM from August through October.

[3] *Wirth* [1991, 1993] studied this fundamental ozone asymmetry by assuming, *a priori*, a planetary wave one thermodynamic structure in the linearized stationary ozone continuity equation. He found that both vertical and horizontal advection substantially contribute to the total ozone perturbation. High column ozone amounts coincided with warm lower stratospheric temperatures in this wave one asymmetry. Other studies of the relationship between the standing wave, jet, and ozone in the SH extratropical stratosphere include those by *van Loon and Jenne* [1972], *Hartmann* [1977], *Mechoso and Hartmann* [1982], *Shiotani and Hirota* [1992], *Randel* [1987], *Randel et al.* [1987], *Newman and Randel* [1988], *Shiotani et al.* [1993], *Aoki et al.* [1996], and *Hio and Yoden* [2005, 2007]. This body of work, however, does not address the underlying cause of the geographical position of the ozone maximum or of the seasonal intensification and eastward migration of the OM from August through October.

[4] This midlatitude ozone asymmetry in the SH winter and spring has important implications for the distribution of radiative heating [*Crook et al.*, 2008] and planetary wave

[1]Department of Atmospheric and Oceanic Sciences, University of Wisconsin-Madison, Madison, Wisconsin, USA.

0148-0227/10/2009JD012883

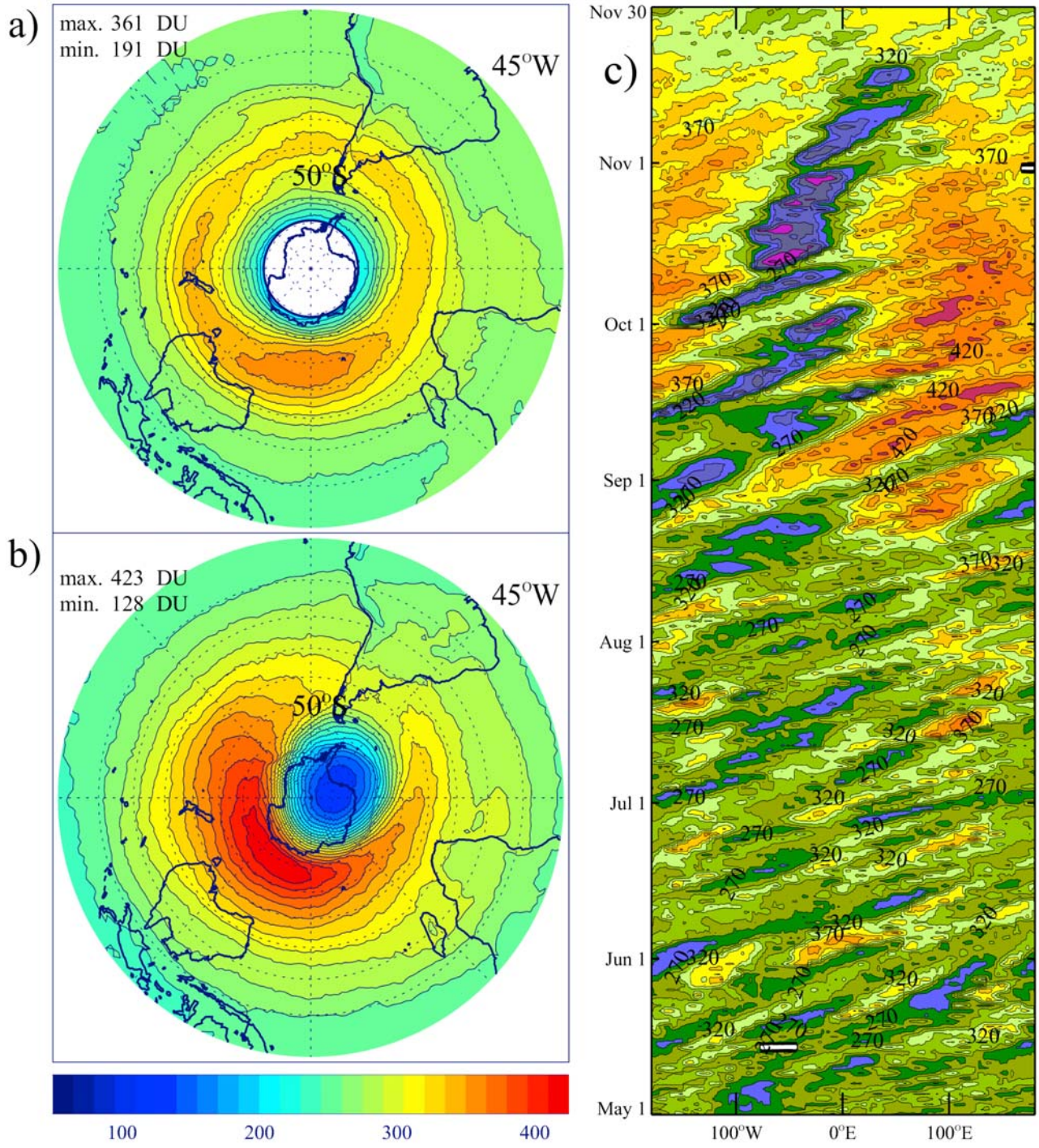

Figure 1. Monthly mean column ozone from the Total Ozone Mapping Spectrometer (TOMS) for (a) August and (b) October 2000, contour interval 15 DU, and (c) longitude-time section of column ozone at 55°S during May 1 November 30, 2000, contour interval 25 DU. The color bar shows low column ozone amounts in blue ranging to high amounts in red.

propagation [*Nathan and Cordero*, 2007]. Moreover, the anthropogenic ozone hole in October is usually displaced toward the South America/Atlantic sector, away from the OM in the Australian sector (Figure 1b). Since the OC and ozone hole are intimately linked as parts of a planetary wave pattern, a better understanding of the dynamics underlying the OM would aid understanding of the variability of the ozone hole [e.g., *Solomon et al.*, 2005; *Grytsai et al.*, 2007]. It will be shown that the primary changes in column ozone from August to October amount to an eastward rotation and amplification of the wave one ozone hole/ozone maximum pattern. It is also of interest to better understand the relationship

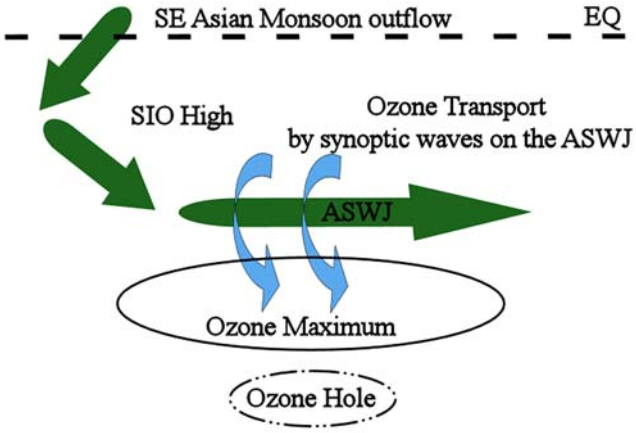

Figure 2. Idealized sketch of the relationship between outflow from Southeast Asian tropical convection in the upper troposphere and lower stratosphere, the anticyclone system over the southern Indian Ocean (SIO High), the Australian Subtropical Westerly Jet (ASWJ), the column ozone maximum poleward of the jet, and the Antarctic ozone hole.

between anthropogenic changes in ozone and greenhouse gases and dynamical feedbacks [*Butchart et al.*, 2006; *Eyring et al.*, 2006; *Garcia and Randel*, 2008]. This is becoming increasingly important in attempting to understand dynamical relationships between phenomena such as the observed strengthening and poleward migration of the SH westerly jet, and ozone hole-induced delayed warming of Antarctica [e.g., *Randel and Wu*, 1999; *Polvani and Kushner*, 2002; *Gillet and Thompson*, 2003; *Thompson et al.*, 2005].

[5] The present work employs distributions of ozone and meteorological fields to show the relationship between tropical convection and fundamental climatological structures in the extratropical lower stratosphere during August to October in the SH winter to spring transition. The existence of intense tropical convection in Southeast Asia and Indonesia during SH winter and spring modulates several key dynamical processes which contribute to the OM. It is argued that the following three dynamical processes are a direct result of seasonal changes in the distribution of tropical convection.

[6] 1. Tropical convective outflow into the upper troposphere and lower stratosphere (UTLS) over the southern Indian Ocean controls the location of the subtropical anticyclone over the SIO and of the Australian subtropical westerly jet (ASWJ; Figure 2).

[7] 2. Synoptic Rossby waves breaking on this jet transport ozone into the OM, which lies just poleward of the jet (Figure 2). From August to October an eastward shift and contraction of tropical convection leads to an increased Australian High in the UTLS, an eastward shift in the Australian jet, and an amplification and eastward shift of the ozone maximum.

[8] 3. The UTLS anticyclones in the southern Indian Ocean sector influence the extratropical longwave pattern. From August to October these anticyclones interact with traveling wave two ridges, which stall in the Australian sector. These ridges are rich in ozone and contribute to the eastward shift of the OM. As the convection shifts eastward the Australian High and midlatitude wave one ridge amplify and shift eastward.

[9] An interesting corollary of the effects of tropical convection is that the north/south asymmetry in the strength and location of the subtropical anticyclones leads to a chemical transport pathway in the UTLS which extends from the NH summer stratosphere southwestward across Indonesia and into the SH winter stratosphere. This pathway transports NH summer stratospheric air across Indonesia, where it mixes extensively with air detrained from tropical convective complexes, arriving 1–2 weeks later near the entrance to the ASWJ. The NH summer stratospheric ozone-rich air is diluted severely by ozone-poor tropical tropospheric air, so that the air arriving over the SIO in the UTLS contains low amounts of ozone. This chemical transport pathway is documented with trajectory analysis.

[10] The dynamical processes underlying processes 1–3 will be explored in monthly means and a synoptic case study from August 2000. The ozone and meteorological fields and analysis methods are described in section 2. The statistical significance of changes in monthly mean column ozone is discussed in section 2.1. Section 3 introduces the three basic processes described above, in the context of the year 2000. A 27-year climatology of Rossby wave breaking statistics for SH winter is shown in section 3.3, which illustrates the relationship between the OM and synoptic Rossby wave breaking, which causes poleward and downward ozone transport near the Australian westerly jet. This climatology also depicts the distribution of zonal mean wind and potential vorticity during the SH winter for dynamical discussion.

[11] A case study from August 2000 is described in section 4, which serves to illustrate synoptic structures associated with the OM, including the relationship between synoptic and planetary waves in the midlatitude lower stratosphere, and the interaction between the SIO high and a stalled planetary wave ridge. The interhemispheric chemical transport pathway from the boreal summer lower stratosphere to the austral winter lower stratosphere is highlighted in section 4. It extends from the boreal summer RWB regime northeast of the Tibetan High, across the equator, and around the SIO anticyclone into the Australian jet.

[12] Section 5 begins with a ten-year climatology of winds and geopotential heights at 150 hPa during August and October. The growth of the Australian High and eastward retreat of the OM are highlighted, as is the zonal contraction of the Australian jet. A momentum budget centered on the SIO shows that export of angular momentum from tropical convection is clearly linked to the entrance of the Australian westerly jet. This section is completed with a discussion of the planetary wave pattern in the 10-year monthly means, which are directly linked to the UTLS anticyclones over the southern Indian Ocean.

[13] Convective outflow pulses modulate the location of subtropical high pressure systems in the UTLS over the southern Indian Ocean. *Rogal et al.* [2010] focus on the relationship between SIO highs and synoptic ozone maxima, which occur in the troughs immediately poleward and eastward of SIO anticyclones, with subsequent eastward dispersion of ozone in the westerly jet. The influence of the El Niño–Southern Oscillation (ENSO) on midlatitude column ozone and on the tropical/extratropical planetary wave relationship are described in *Hitchman and Rogal* [2010]. Here

we focus on the effects of seasonal changes in tropical convection on the Australian westerly jet and planetary wave pattern radiating into the SH.

2. Data and Analysis

2.1. Global Ozone and Meteorological Fields

[14] Total Ozone Mapping Spectrometer (TOMS) column ozone, and 3D global ozone from the NASA Global Modeling and Analysis Office (GMAO) Goddard Earth Observing System-4 (GEOS-4) data [*Stajner et al.*, 2001, 2004, 2006] were used to describe ozone variability. GEOS-4 data were produced for the years 1998, 2000, and 2004 by assimilating meteorological data and ozone from the Solar Backscatter Ultraviolet Instrument on a 2° × 2.5° grid.

[15] Daily data from the European Centre for Medium-Range Weather Forecasting (ECMWF) [*Hollingsworth et al.*, 1986; *Kallberg et al.*, 2005], National Center for Environmental Prediction (NCEP) [*Kalnay et al.*, 1996], and the United Kingdom Meteorological Office (UKMO) [*Swinbank and O'Neill*, 1994] were used to depict general circulation structures and statistics. We have examined the behavior of the OM and the SH general circulation for each year during 1982–2004 and the GEOS-4 data for 1998, 2000, and 2004. The year 2000 was selected for this work. Although La Nina conditions prevailed during August–October 2000, which caused a westward shift [*Hitchman and Rogal*, 2010], the seasonal amplification and eastward migration from August through October occurred in 2000, as it does in every year examined.

[16] The Langley Research Center isentropic trajectory code [*Pierce and Fairlie*, 1993] was used in conjunction with ECMWF data to illustrate the interhemispheric cross-equatorial transport pathway at 350 K, which lies near 14 km altitude or 150 hPa in the tropics.

[17] Monthly mean outgoing longwave radiation plots from 2000 were obtained from the NOAA ESRL Physical Sciences Division to show the change in the distribution of convection from August through October.

[18] Montgomery stream function (M) and potential vorticity (PV) were calculated and interpolated to isentropic levels spaced 10–50 K apart on a 2.5° × 5° grid [*Andrews et al.*, 1987] (1 PVU = 10^{-6} K m^2 kg^{-1} s^{-1}). On potential temperature surfaces the geostrophic wind flows parallel to $M = C_pT + \Phi$, where T is temperature and Φ is geopotential. Examples of M on theta surfaces from UKMO data are shown in the case study.

[19] The geographical distribution of Rossby wave breaking (RWB) provides useful information about the distribution of irreversible transport. An RWB event occurs when the meridional gradient of PV, P_y, is negative, that is when PV contours fold over in the x − y plane. This is usually accompanied by folding over of isentropic surfaces in the vertical. *Hitchman and Huesmann* [2007] present seasonal climatological distributions of P_y, together with the distribution of RWB frequency and strength. *Hitchman and Huesmann* [2009] discuss the effects of the stratospheric QBO on the jet structure and distribution of RWB. Here a 27-year climatology of RWB statistics using NCEP data for the period 1979–2005 is shown for June–July–August (JJA).

[20] In order to emphasize the continuity of wave activity from a UTLS SIO high to a stalled stratospheric ridge it is useful to multiply eddy geopotential height, Z', by $e^{-z/2H}$ (see Figure 14). This makes it easier to compare the magnitude of wave activity at different altitudes and emphasizes the upward influence that an anticyclone in the UTLS over the SIO can have on the extratropical planetary wave pattern. This scaling emerges from linear Rossby wave theory and conservation of wave activity, $A \propto \rho q'^2 \propto \rho Z'^2$, where ρ is atmospheric density, and q' is quasi-geostrophic potential vorticity. Since $\rho \propto p \propto e^{-z/H}$, $Z' \propto e^{z/2H}$, and for a constant distribution of A, $e^{-z/2H}\,Z'$ would be constant with altitude. Upward diminution of this quantity would be consistent with absorption of wave activity along the path.

2.2. Statistical Significance of Monthly Mean Column Ozone Changes

[21] The amplification and eastward migration of the OM from August to October and its statistical significance are shown in auxiliary material Figure S1.[1] The first column shows monthly mean composites of available TOMS column ozone over the 22-year record 1982–2004 for the months of August, September and October. The ozone maximum near 50°S is located near 110°E in August but migrates to near 140°E and is noticeably stronger in October. This seasonal eastward shift is seen in Figure 1c for the year 2000.

[22] The second column in Figure S1 shows the changes in column ozone from August to September, September to October, and August to October. The primary change from August to September is an increase in the OM directly south of Australia. The primary change from September to October is an increase in column ozone in the band 50–70°S in the Pacific sector, centered on the Date Line. These changes constitute the eastward shift of the OM.

[23] The third column in Figure S1 shows the standard deviation of monthly mean column ozone for the 22 years. Interannual variability of monthly mean column ozone increases markedly into the polar vortex, near the edge of the ozone hole where the gradient is steepest. Standard deviations in the polar vortex increase from August to October, especially south of South Africa, with much of this variability associated with ENSO [*Hitchman and Rogal*, 2010].

[24] Student's T-statistic

$$T = \frac{X - Y}{\sqrt{\sigma_X^2/N + \sigma_Y^2/M}} \tag{1}$$

was used to assess the probability that two sample populations have meaningfully distinct averages, X and Y, with variances σ_X^2 and σ_Y^2, and degrees of freedom N and M. For differences among the monthly means, $N = M = 22$, corresponding to the number of seasons used in the TOMS record. Results are presented as percent statistical significance, where 97.5% indicates only a 2.5% chance that differences are purely random.

[25] Statistically significant differences between monthly means exceeds 99% over the vast majority of the SH (green in Figure S1). Values between 99 and 97.5% are shown in yellow, while values less than 97.5% are shown in red. Near a zero contour for monthly ozone differences or near large standard deviations, (1) indicates that the T-score should

[1] Auxiliary materials are available in the HTML. doi:10.1029/2009JD012883.

be low. All regions in column four showing statistical significance less than 99% can be traced to regions of small differences in column two and regions of large variability in column three. The increases seen in the high latitude Pacific sector from August to October are therefore highly statistically significant and are a reliable feature of the SH winter to spring transition.

3. Monthly Mean Structure for 2000

[26] In this paper the fundamental cause of the OM and its intensification during the austral winter to spring transition is explored. The explanation is found by connecting processes which are usually treated separately in the literature: the relationship between tropical convection and subtropical westerly jets, ozone transport by synoptic waves breaking on the jets, and ozone transport by stratospheric planetary waves. Southeast Asian monsoon tropical convective outflow influences the distribution of extratropical column ozone by determining the location of the Australian subtropical westerly jet (dynamical process (1); Figure 2). The OM lies immediately poleward of the Australian jet, coinciding with warm temperatures and a poleward Rossby wave breaking surf zone (dynamical process (2); Figure 2).

3.1. Tropical Convection and Subtropical Westerly Jets

[27] *Nogues-Paegle and Zhen* [1987] showed that Southeast Asian monsoon outflow during boreal summer supplies westerly zonal momentum to the Australian westerly jet. Strengthening of this jet occurs with bursts of deep convection over Southeast Asia and Indonesia. The coupling between the forcing region and the rotational wind response extends through the tropics into the winter hemisphere. When projected onto normal modes, convective bursts create westward flow in the UTLS as part of a Kelvin wave, then southward flow as part of a large inertia-gravity wave, then as short Rossby waves modulating the Australian jet, then as tall Rossby waves modulating the polar night jet. This is consistent with the idea that tropical convection can modulate stratospheric jets via outflow in the UTLS and radiation of planetary waves [*Dickinson*, 1971]. *Berberry et al.* [1992] concluded that the Australian westerly jet and polar night jet act as waveguides for disturbances emanating from the southern Indian Ocean.

[28] *Nogues-Paegle and Mo* [1988] found that tropical convective divergence maximum for these events lies ~50° east of jet accelerations. The effects of latent heating maxima are noticed within 2–4 days in the SH subtropics, and are fully established by 6 days. Week to week variations in divergent outflow are intimately related to variations in convection [*Kiladis and Mo*, 1998; *Renwick and Revell*, 1999] and to the extent of the Tibetan High [*Randel and Park*, 2006].

[29] The energetic tropical circulation is intrinsically zonally asymmetric, being composed of local monsoon circulations linked to the distribution of continents [*Bjerknes et al.*, 1933; *Krishnamurti et al.*, 1973; *Johnson*, 1989]. The contrast between the hot Asian land mass and cool southern Indian Ocean creates a unique configuration in the general circulation of the planet. During boreal summer most of the zonal mean meridional mass flow across the equator in the upper UTLS occurs over the Indian Ocean [*Newell et al.*, 1972]. This basic structure can be understood in terms of steady-state solutions to tropical tropospheric heating anomalies associated with convective centers over Southeast Asia and Indonesia [e.g., *Gill*, 1980; *Hendon and Hartmann*, 1982; *Rodwell and Hoskins*, 2001]. Near the equinoxes convection tends to be centered over Indonesia. During austral winter the center of convection migrates northwestward toward the Himalayas. During austral spring the convection migrates southeastward toward Indonesia [*Liebmann and Hartmann*, 1982].

[30] This shift from August to October 2000 is shown in Figure 3. During August outgoing longwave radiation is low throughout Southeast Asia and the western tropical Pacific (Figure 3a). Blue regions in the tropics indicate cold high clouds associated with deep convection. Its zonal extent during August is ~100° of longitude, as indicated by the thick gray arrow. Note also the regions of tropical convection in August just north of the equator in Africa and over the Gulf of Panama. As the sun shines more directly on the SH during October, convection migrates southeastward to Amazonia, Central Africa, and Indonesia (Figure 3b). The zonal extent of the Indonesian convection in October is ~60° of longitude, a significant zonal contraction. It will be shown that the change in the shape of convection over Southeast Asia and Africa are directly related to changes in anticyclones over the South Indian Ocean High system and to changes in the zonal extent of the Australian westerly jet, and hence the sharpness and location of the OM.

[31] Figures 4 and 5 show ECMWF 150 hPa wind and geopotential height, 150 hPa eddy geopotential height, 150 hPa zonal wind, 100 hPa temperature, and TOMS column ozone averaged during July–August–September 2000. Anticyclonic flow around the Tibetan High crosses Indonesia, and curves clockwise around the SIO high into the entrance of the Australian westerly jet (Figures 4a and 4b). This seasonal flow structure was shown by *Krishnamurti et al.* [1973], *Vincent and Silva Dias* [1998] and *Annamalai et al.* [1999]. The eddy height field in Figure 4b shows a planetary Rossby wave train emanating from the SIO High southeastward into the extratropical lower stratosphere. This emphasizes the influence that tropical convection can have on the extratropical planetary wave pattern in the UTLS [*Dickinson*, 1971; *Sardeshmukh and Hoskins*, 1988].

[32] The strong southwestward current across Southeast Asian into the SIO at 150 hPa (Figure 4a) flows amidst the tops of convective complexes for a distance of 5,000–10,000 km (Figure 3). Most of the air in this current that reaches the SIO was tropical boundary layer air detrained into the UTLS. This air has high angular momentum and is the primary cause of the entrance to the Australian westerly jet. The momentum budget of this jet will be explored quantitatively in section 5.2.

3.2. Relationship Between the Australian Jet and Ozone Maximum

[33] Immediately poleward of the Australian subtropical westerly jet (ASWJ; Figure 5a) lies a region of warm air at 100 hPa (Figure 5b), also shown by *Hurrell et al.* [1998], which is coincident with high column ozone in the OM (Figure 5c). *Newman and Randel* [1988] documented this high spatial correlation between lower stratospheric temperature and column ozone for October 1979–1986. This strong correlation is the result of regular poleward and downward

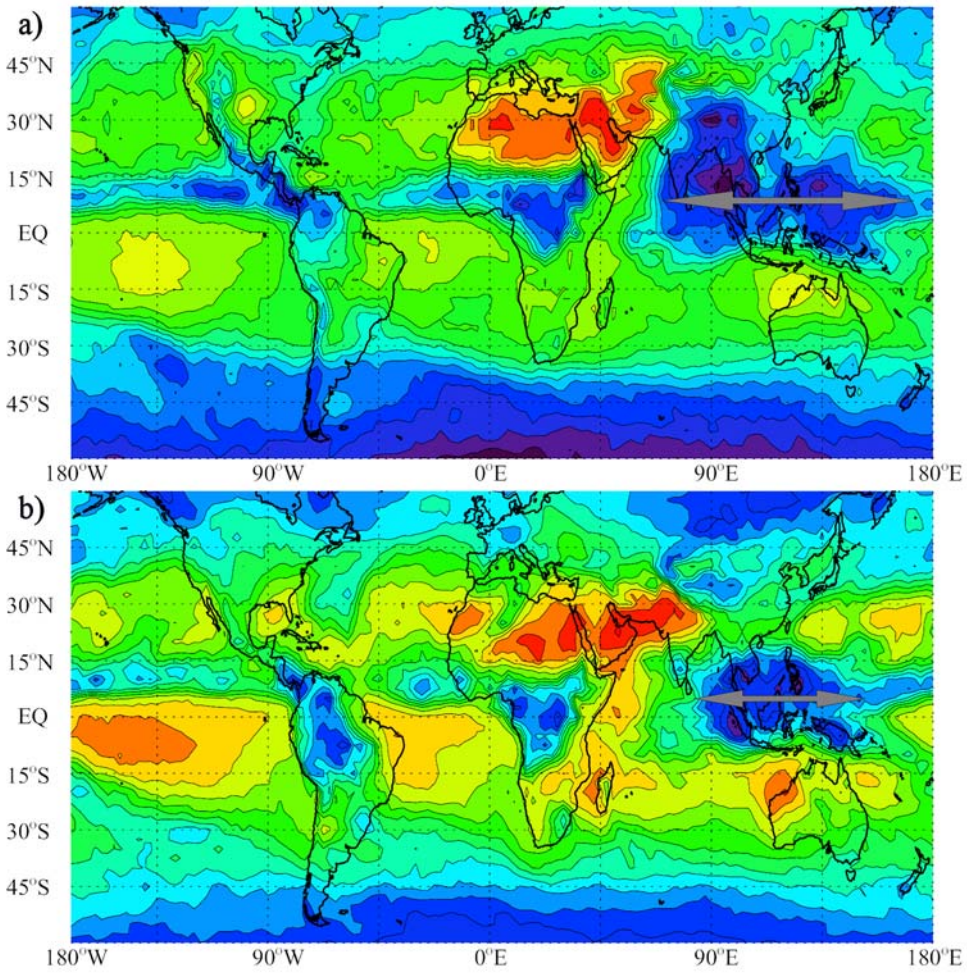

Figure 3. Monthly mean outgoing longwave radiation, contour interval 10 W m^{-2}, during (a) August, range 0–160 W m^{-2}, and (b) October 2000, range 20–170 W m^{-2}. Blue colors indicate cold cloud tops, while red colors indicate warm surfaces. Note southeastward shift and zonal contraction of the region of deep convection over Southeast Asia from August to October as indicated by the thick gray arrows. Values were obtained from the NOAA Earth System Research Laboratory.

Lagrangian circulation within synoptic waves modulating the jet [*Kida*, 1977; *Wallace*, 1978]. This Stokes drift results from the eddy amplitude maximum near the jet axis. Absorption of synoptic Rossby waves and inertia-gravity waves radiating into the lowest stratosphere from evolving tropospheric disturbances [*O'Sullivan and Dunkerton*, 1995] constitutes an easterly body force, which implies a poleward and downward flow [*Haynes et al.*, 1991]. High resolution observational studies with dropwinsondes [*Shapiro*, 1980] highlight upper level frontogenesis and a Sawyer-Eliassen circulation transporting stratospheric air poleward and downward around the jet and into the troposphere [*Keyser and Shapiro*, 1986].

[34] *Hudson et al.* [2003] emphasize the subtropical westerly jets as separating a tropical regime with low column ozone from a midlatitude regime with high column ozone. A comparison of Figures 1 and 5 shows the striking spatial relationship between the OM and the Australian westerly jet on its poleward flank, where the tropopause altitude is significantly lower. A schematic of this relationship is shown in Figure 2, with transparent curved arrows indicating the poleward and downward transport by synoptic waves breaking on the Australian westerly jet. It should be emphasized that the pathway of ozone from its production region in the subtropical stratosphere to the lowest stratosphere poleward of the Australian jet is long and complex [e.g., *Sato et al.*, 2009]. In general, transport of ozone-rich tropical PV air into the midlatitudes leads to high ozone at the base of planetary wave ridges [*Harvey et al.*, 2004].

3.3. RWB Surf Zone and the Ozone Maximum

[35] In order to highlight the spatial coincidence of synoptic Rossby wave breaking and the ozone maximum, a 27-year seasonal mean distribution of RWB statistics for June–July–August (JJA) at 360 K (~150 hPa) is shown in Figure 6. PV gradient maxima highlight the Australian westerly jet near 30°S and the base of the polar night jet near 55°S. In conjunction with the planetary wave pattern seen in Figure 4a, the polar night jet is strong over the Indian Ocean and angles poleward as it diminishes south of Australia. The Australian

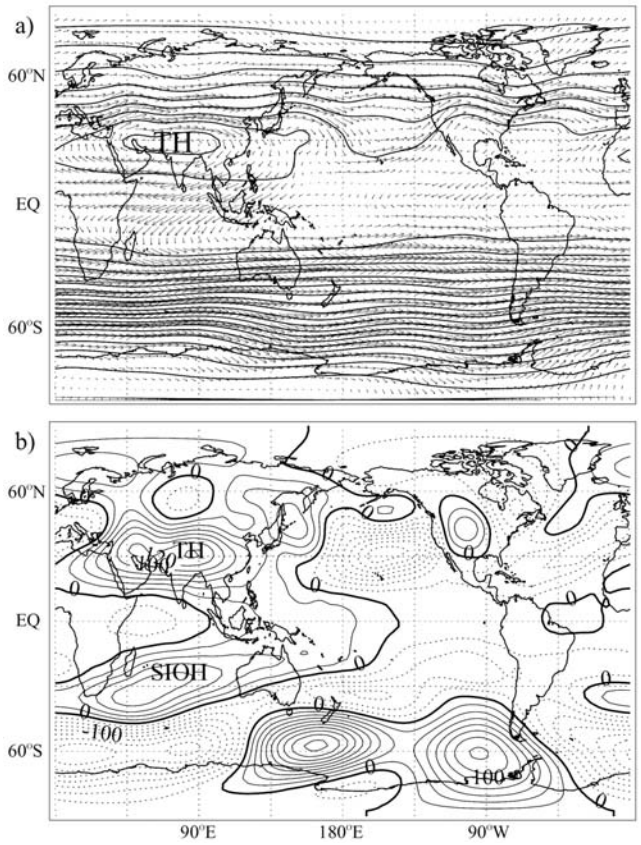

Figure 4. ECMWF July August–September 2000 average 150 hPa (a) geopotential height, contour interval 100 m, and wind vectors, maximum length 50 m/s, and (b) eddy geopotential height, contour interval 20 m. The Tibetan High (TH) north of the equator and the southern Indian Ocean High (SIOH) south of the equator lie poleward and westward of Southeast Asian convection. Note the propagation of a planetary wave train from the SIOH toward high latitudes.

jet near 30°S begins over the SIO west of Australia, then extends eastward toward Chile. Immediately poleward of the Australian jet and equatorward of the diminishing polar night jet is a synoptic wave surf zone, where RWB is common (large circles) and moderately strong (green). The synoptic RWB regime near 45°S at 360 K coincides geographically with the distribution of column ozone (Figures 1 and 5c). This pattern is also strikingly similar to the pattern of stratosphere to troposphere flux in model diabatic heating calculations [*Olsen et al.*, 2004].

[36] The vertical distribution of RWB during JJA is shown in Figure 7, with frequency (circle size) and breaking strength (circle color) superimposed on zonal mean zonal winds (Figure 7a) and on zonal mean PV gradient, P_y (Figure 7b). The synoptic RWB surf zone poleward of the Australian jet blends seamlessly with the planetary RWB surf zone equatorward of the polar night jet [*Hitchman and Huesmann*, 2007]. The planetary wave surf zone spans the broad minimum in P_y from the polar night jet near 60°S to the equator (Figure 7b). Vertical propagation of EP fluxes in this waveguide was originally studied by *Randel et al.* [1987]. The vertical coherence of planetary wave phase in this regime was shown by *Hurrell et al.* [1998]. Since ozone concentration maximizes in the layer 10–30 km, this surf zone controls ozone transport through interactions between upwardly evanescent synoptic waves breaking poleward of the Australian jet and planetary waves breaking equatorward of the polar night jet.

3.4. Radiation of Planetary Wave Energy Into the Southern Hemisphere

[37] The 150 hPa geopotential height anomalies for July–August–September 2000 exhibit a teleconnection between

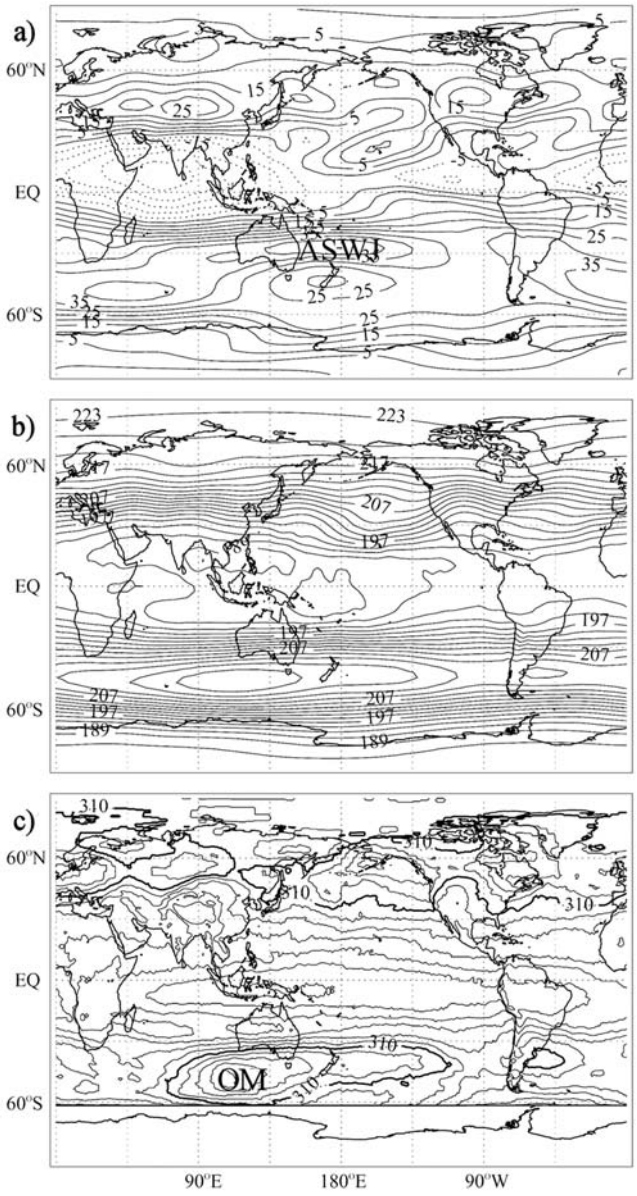

Figure 5. ECMWF July August–September 2000 average (a) 150 hPa zonal wind speed, contour interval 5 m/s, and (b) 100 hPa temperature, contour interval 2 K, with (c) TOMS column ozone, contour interval 10 DU, with the 310 DU contour emphasized to show the SH ozone maximum in the warm anomaly directly south of the Australian subtropical westerly jet (ASWJ).

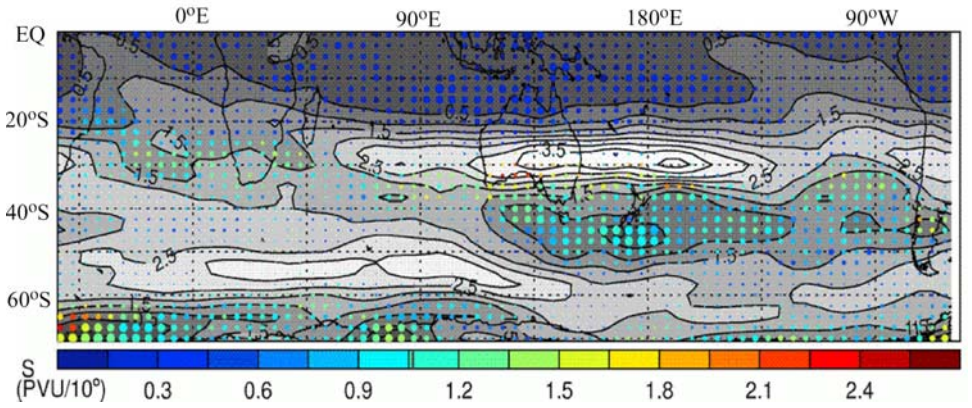

Figure 6. NCEP 360 K June–July August 27-year average PV gradient (contour interval 0.5 PVU per 10° latitude, also shaded from small values in dark gray to large values in white), PV gradient reversal frequency indicated by circle size (maximum 35 reversals per 100 days), and PV gradient reversal strength indicated by color (see color bar). The maximum in PV gradient indicates the Australian Subtropical Westerly Jet. Note the synoptic Rossby wave breaking "surf zone" on the poleward side of this jet characterized by frequent (large circles) and moderately strong (green circle color) PV gradient reversals.

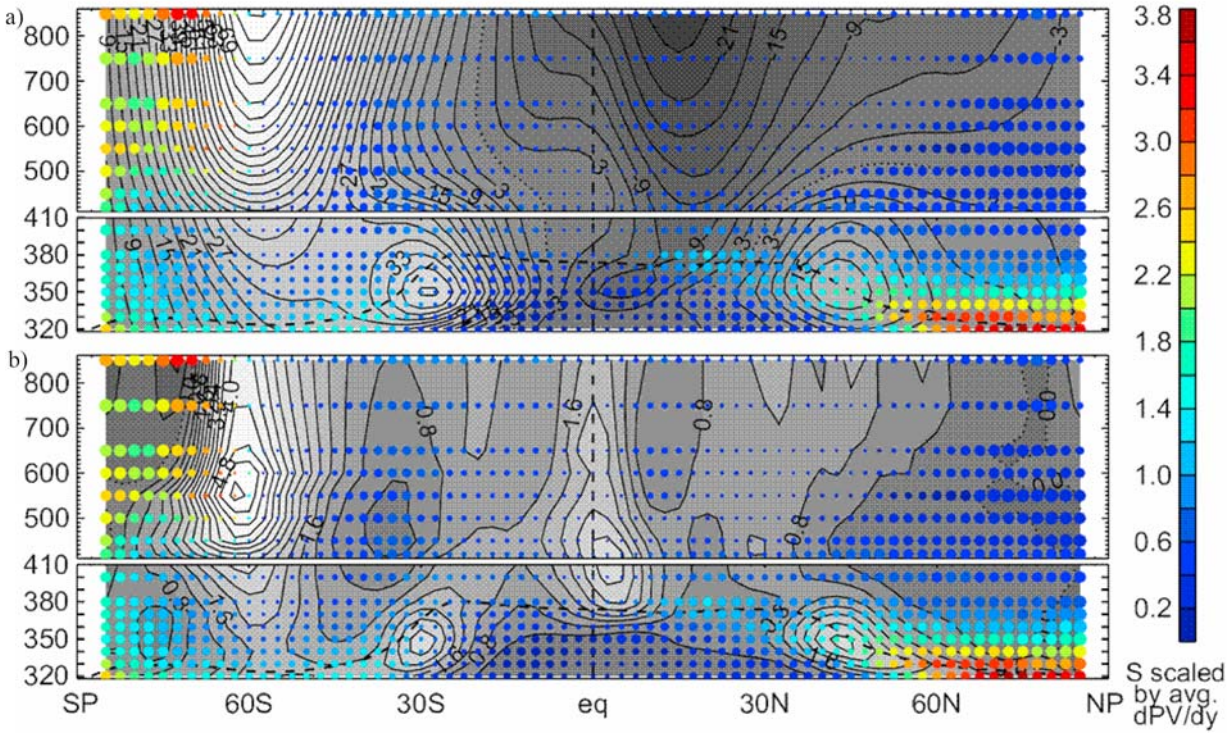

Figure 7. NCEP June–July August 27-year average zonal mean (a) zonal wind, contour interval 3 m s^{-1}, with zero contour dashed, and shading ranging from −25 m s^{-1} (dark gray) in the subtropical stratospheric easterly jet to 80 m/s (white) in the polar night jet, and (b) PV gradient normalized by the global mean at each level, contour interval 0.3, ranging from small values in the summer polar stratosphere (dark gray) to large values in the polar night jet (white), with PV gradient reversal frequency indicated by circle size (maximum 35 reversals per 100 days), and PV gradient reversal strength indicated by the color bar, ranging from weak (blue) to strong (orange). The region of moderate RWB poleward of the Australian subtropical westerly jet and equatorward of the polar night jet coincides with the ozone maximum.

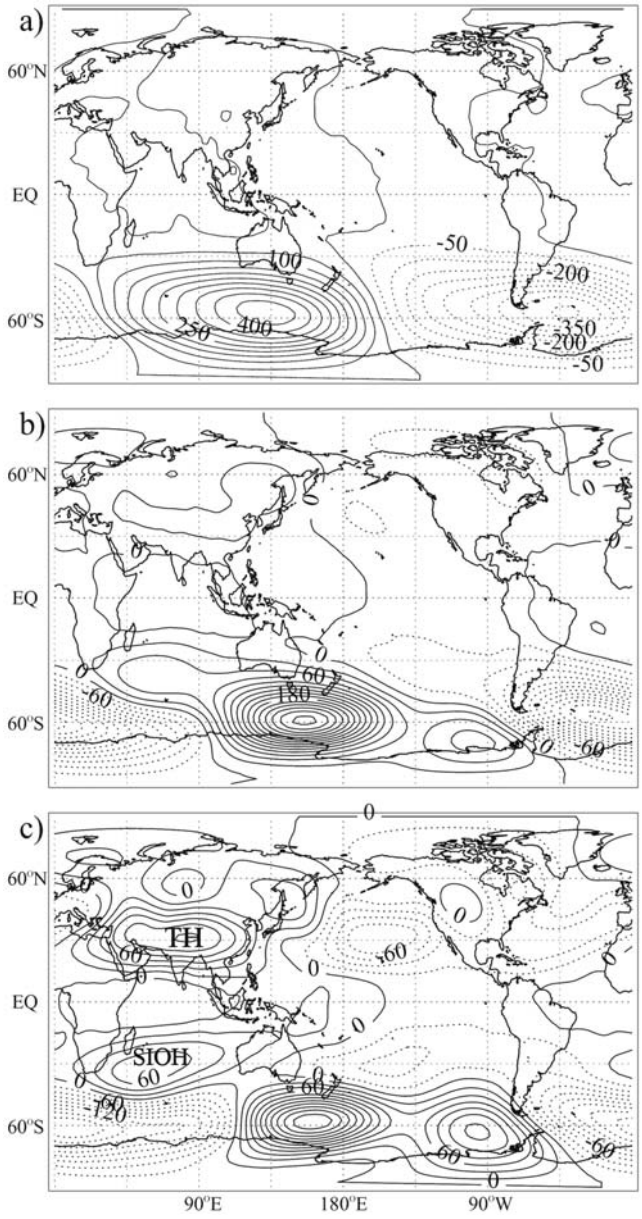

Figure 8. ECMWF July August–September 2000 average eddy geopotential height at (a) 10 hPa, contour interval 50 m, (b) 50 hPa, contour interval 20 m, and (c) 100 hPa, contour interval 20 m, showing the upward evanescence of the Tibetan High (TH) into summer easterlies and upward influence of Rossby wave activity emanating from the SIO anticyclones (SIOH) into winter westerlies. These may be compared with the 150 hPa level shown in Figure 4b.

the southern Indian Ocean in the tropical UTLS (Figure 4b) and a barotropic anticyclone south of Australia in the winter stratosphere (Figure 8). At 100 hPa a pair of anticyclones is seen westward and poleward of Indonesian convection, the Tibetan High and the SIO High. The SIO high extends diagonally southwestward from New Guinea to South Africa (Figure 8c). The southward flow field in Figure 4a exhibits counter-clockwise curvature centered near the axis of maximum heights. The maximum in column ozone (45°S, 110°E; Figure 5c) lies immediately poleward and downstream of this anticyclonic anomaly. Poleward and downstream of the SIO high lies a trough, then a long ridge near 60°S (Figure 4b). This pattern is consistent with Rossby wave energy radiating from the tropics [*Sardeshmukh and Hoskins*, 1988].

[38] Figure 7a shows that westerly winds increase poleward from 10°S into the winter stratosphere, but that easterlies occupy the middle and upper summer stratosphere. Consistent with the Charney - Drazin criterion, Rossby wave energy associated with quasi-stationary monsoon anticyclones in the subtropical UTLS propagates readily from the tropics into winter stratospheric westerlies, but critical surfaces prevent wave activity from propagating into summer stratospheric easterlies. This hemispheric differential filtering begins to be seen at 50 hPa (Figure 8b). The Tibetan High does not penetrate very far into the easterlies, but the SIO High and extratropical ridge in the winter westerlies are robust, yet merged into one elongated ridge. Note the upward amplification of the ridge south of Australia, while that near South America shrinks with altitude (Figures 8b and 8c).

[39] At 10 hPa (Figure 8a) the merged anticyclone, a blend of the upward-extending SIOH and stalled stratospheric planetary wave ridge, extends from the South Pole to Australia and 30°E to 150°W. This position is similar to the position of stalled ridges observed by *Mechoso et al.* [1988], an aspect which will be explored further in the next section. The Charney - Drazin criterion also holds that strong westerly winds select for longer zonal scales. An upward transition to a wave one pattern in the strong polar night jet (Figure 7a) is seen in Figure 8. Considering eddy geostrophic flow around the anticyclonic anomalies at 10 hPa and 50 hPa (Figures 8a and 8b), flow from the subtropical South Atlantic makes its way around the poleward side of the high. This structure can contribute to the seasonal transport of ozone out of the sunlit tropics into the poleward side of the ridge, ultimately becoming available for convergence into a synoptic wave trough, as shown in the next section.

4. Case Study of 24 August 2000

4.1. Synoptic Relationship Between Ozone and Height Fields

[40] An example of the synoptic structures associated with ozone patterns is shown for 24 August 2000 in Figures 9 and 10. At 150 hPa the subtropical westerly jet separates low column ozone in the tropics from higher amounts in the extratropics (Figures 9a and 9b). Ozone is concentrated in synoptic troughs, with the most prominent concentration in the trough just poleward of the outflow pulse, near 50°S, 90°E (Figure 9b). A meridional section (Figure 10a) shows a striking and characteristic pattern of subsidence into the troposphere near 35–60°S from the ozone maximum near 21 km to well below the tropopause. This deep region of concentrated ozone near 50°S lies in the stratospheric winter surf zone poleward of the Australian jet and equatorward of the polar night jet (Figures 6 and 7).

[41] A zonal section at 47.5°S (Figure 10b) shows that lower stratospheric ozone maximizes (orange) in the layer 70–30 hPa, in the longitude bands 20°W–140°E and 180°W–70°W, at the base of the planetary wave ridges (labeled solid contours). Note the transition from planetary wave to

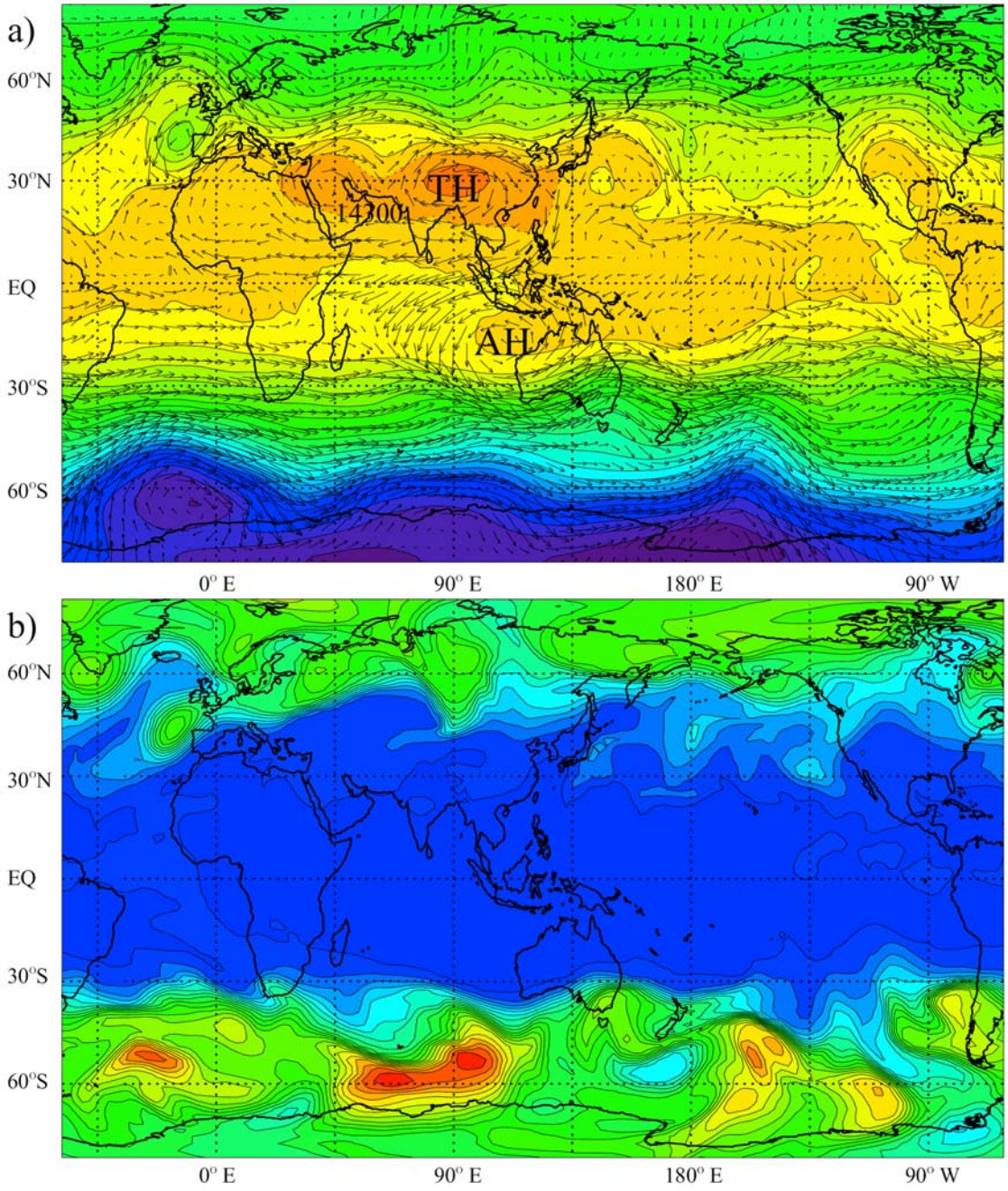

Figure 9. Sections through the ozone transport case study at 1200 UT on 24 August 2000 of (a) ECMWF 150 hPa geopotential height, contour interval 100 m, and wind vectors, reaching 40 m/s just northwest of the Australian High (AH), and south of the Tibetan High (TH), where orange (blue) indicates high (low) geopotential heights, and (b) 150 hPa GMAO ozone mixing ratio, contour interval 50 ppbv, where orange (blue) indicates high (low) ozone mixing ratio.

synoptic scale features in ozone and eddy geopotential height across the UTLS. Note also that in the upper troposphere ozone maxima (orange) occur in synoptic scale troughs (dashed labeled contours). The two "feeder highs" make ozone available for subsidence into the troughs in the UTLS, especially near 90°E (see Figures 9b and 10a). This relationship can also be observed near 160°W and 20°W (compare Figures 9b and 10b).

4.2. Interhemispheric Mixing Pathway

[42] *Rogal et al.* [2010] show some trajectories in a model simulation which spiral down around the polar vortex into an upper tropospheric ozone maximum south of Australia. This pathway into the OM is quite distinct from the cross-equatorial transport pathways which lead into the Australian jet. The cross-equatorial pathway into the jet is shown with isentropic parcel trajectories which arrive at the jet entrance.

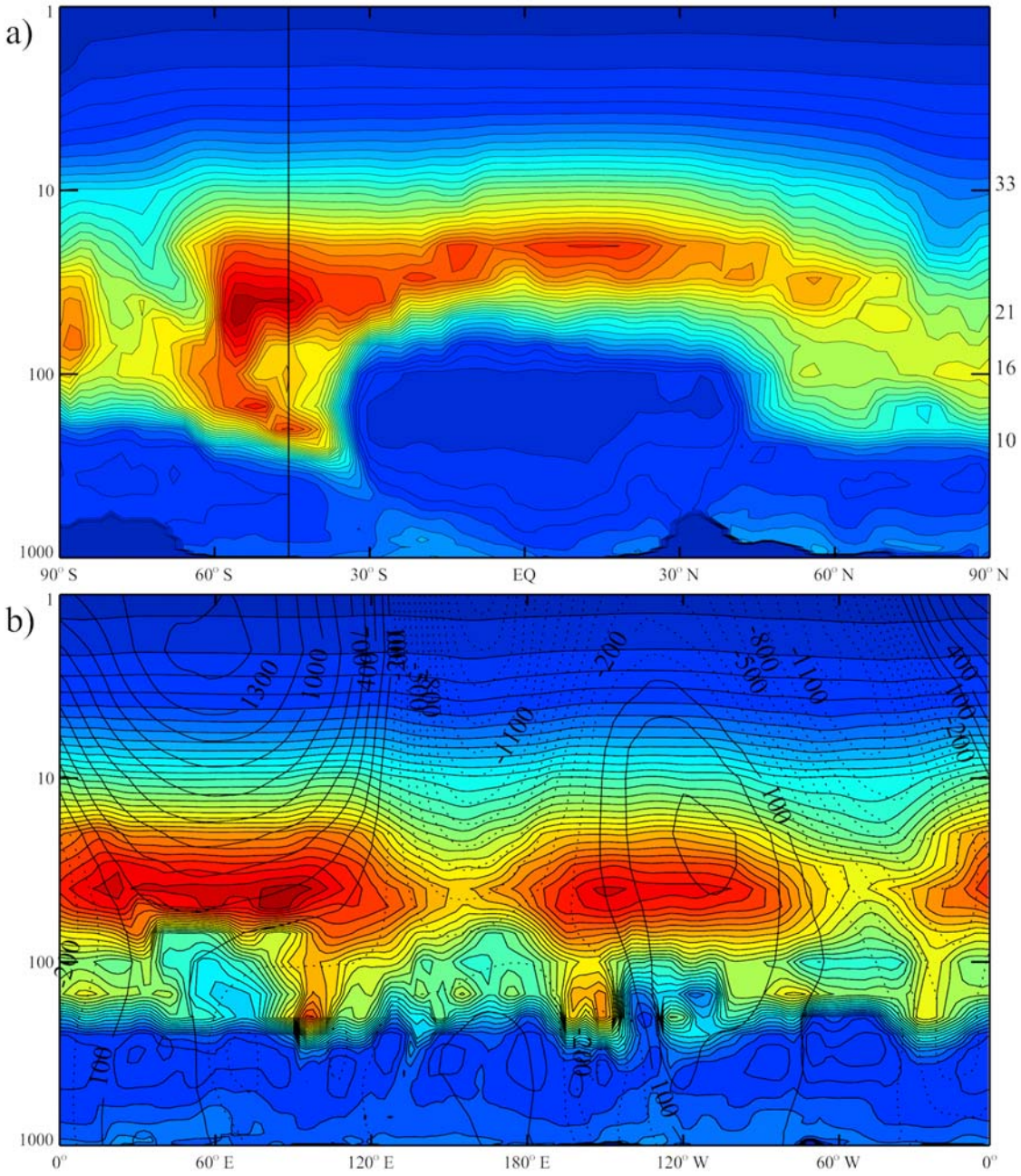

Figure 10. Sections through the ozone transport event at 1200 UT on 24 August 2000: (a) GMAO ozone concentration at 95°E, contour interval 1.5×10^{18} molecules m^{-3}, and (b) eddy geopotential height, solid lines with labels, contour interval 150 m, and GMAO ozone concentration at 47.5°S, indicated in color and thin solid contours without labels, contour interval 1.5×10^{18} molecules m^{-3}. In Figures 10 and 10b, orange (blue) indicates high (low) ozone mixing ratio amounts. In Figure 10a the approximate altitude in km is shown at the right and 47.5°S is indicated with a vertical black line. Note the poleward and downward circulation in midlatitudes in Figure 10a and the coincidence of high ozone values (orange) in the wave two ridges (labeled solid black contours) in the lower stratosphere in Figure 10b. The dashed contour in the upper troposphere near 100°E indicates a synoptic wave trough coincident with high ozone (orange).

A sample of trajectories at 350 K is shown for the case study of 24 August 2000 in Figure 11. The ending locations are positioned successively eastward from the jet entrance to eastern Australia. Each of the eight days is colored separately, with orange the oldest and black the youngest portions of the trajectories. Parcels arriving near the jet entrance at this time (Figure 11a) come from the RWB mixing zone near Japan [*Postel and Hitchman*, 1999] and cross the

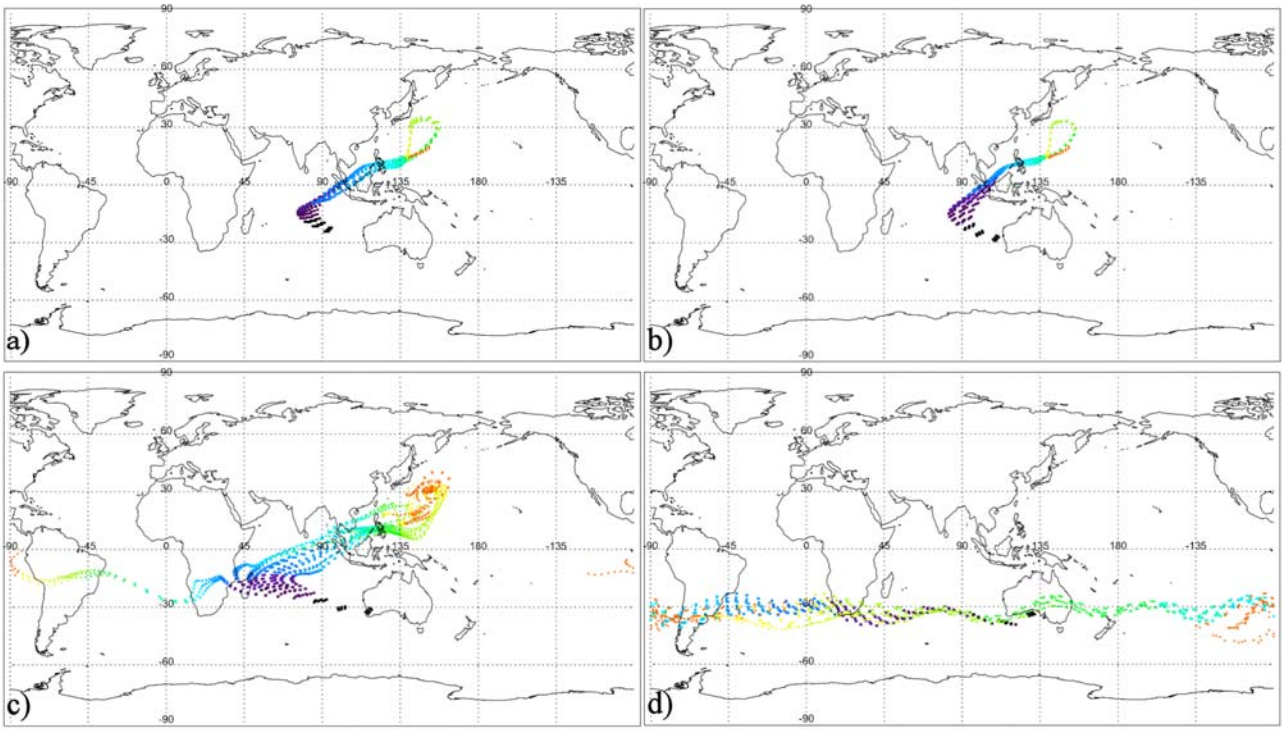

Figure 11. Eight day back-trajectories at 350 K ending on 0000 UT 24 August 2000 at 25°S and longitudes (a) 100°E, (b) 120°E, (c) 130°E, and (d) 140°E, using twice-daily gridded ECMWF data. Locations are plotted every six hours, with color changing from black (less than one day prior to arrival time) to purple (2 days), dark blue (3 days), light blue (4 days), dark green (5 days), light green (6 days), yellow (7 days), and orange (8 days prior).

equator southwestward. A 40 year climatology of radiosonde data at Singapore and Diego Garcia [*Yao*, 1994] (not shown) documents southwestward flow in the layer 10–17 km (~300 − 100 hPa), with the southward component exceeding 5 m/s near 14 km (~150 hPa) during May–October. Parcels arriving farther east in the jet are a mixture of air in the cross-equatorial pathway and air coming from the west in the southern subtropics (Figures 11b and 11c). Parcels appearing in the middle of the jet at this time originated in the subtropical westerlies, making nearly two trips around the globe in 8 days (Figure 11d).

[43] The trajectories in Figures 11a–11c pass through thousands of kilometers of cumulonimbus turrets and anvils (Figure 3), which inject detrained tropical tropospheric air into this pathway. This explains why this pathway is not apparent in maps of ozone (Figure 9b). Since tropical boundary layer air has large planetary angular momentum, this also accounts for how westerly angular momentum is supplied to the Australian jet by "cumulus friction" along this pathway [*Schneider and Lindzen*, 1980].

4.3. Connection Between SIO Highs and Extratropical Ridges

[44] *Quintanar and Mechoso* [1995a] found that the quasi-stationary wave one in dynamical fields in the UTLS is linked to EP fluxes from the tropical Indian Ocean. *Quintanar and Mechoso* [1995b] carried out general circulation experiments with Antarctic topography and concluded that the subtropical wave one pattern is not related to Antarctica. *Renwick and Revell* [1999] showed that blocking events in the Southeast Pacific are associated with synoptic Rossby wave trains emanating from the Australian sector and linked them to anomalous convection events in the tropics. *Newman and Nash* [2005] identified subtropical forcing during austral winter as a key ingredient in the unusual sudden warming that occurred on 24 September 2002.

[45] *Mechoso et al.* [1988] and *Charlton et al.* [2005] summarized the seasonal transition from southern winter to spring as follows. During September the polar vortex is often elongated, with a pair of anticyclones 180° apart, each at a different stage in their life cycle. They tend to form over the SIO, with a life cycle of growth and decay over about 10 days as they migrate eastward. In October the flow regime often changes to a quasi-stationary wave one anticyclone over the Pacific.

[46] An example of the temporal coincidence between amplification of subtropical highs in the SIO UTLS and stalling and amplification of traveling planetary wave ridges in the extratropical lower stratosphere is shown for our case month of August 2000 in Figure 12. Near 360 K (~15 km) at 17°S, quasi-weekly variability of the AH may be seen near 120°E (Figure 12a). Near 700 K (~26 km) at 46°S, planetary scale ridges and troughs may be seen traveling eastward at ~14 m s^{-1} (Figure 12b). The wave two component has zonal wavelength ~14,000 km and period ~10 days, characteristic behavior of the southern winter [*Leovy and Webster*, 1976; *Mechoso and Hartmann*, 1982; *Randel*, 1987]. These finite amplitude regional ridges and troughs project onto

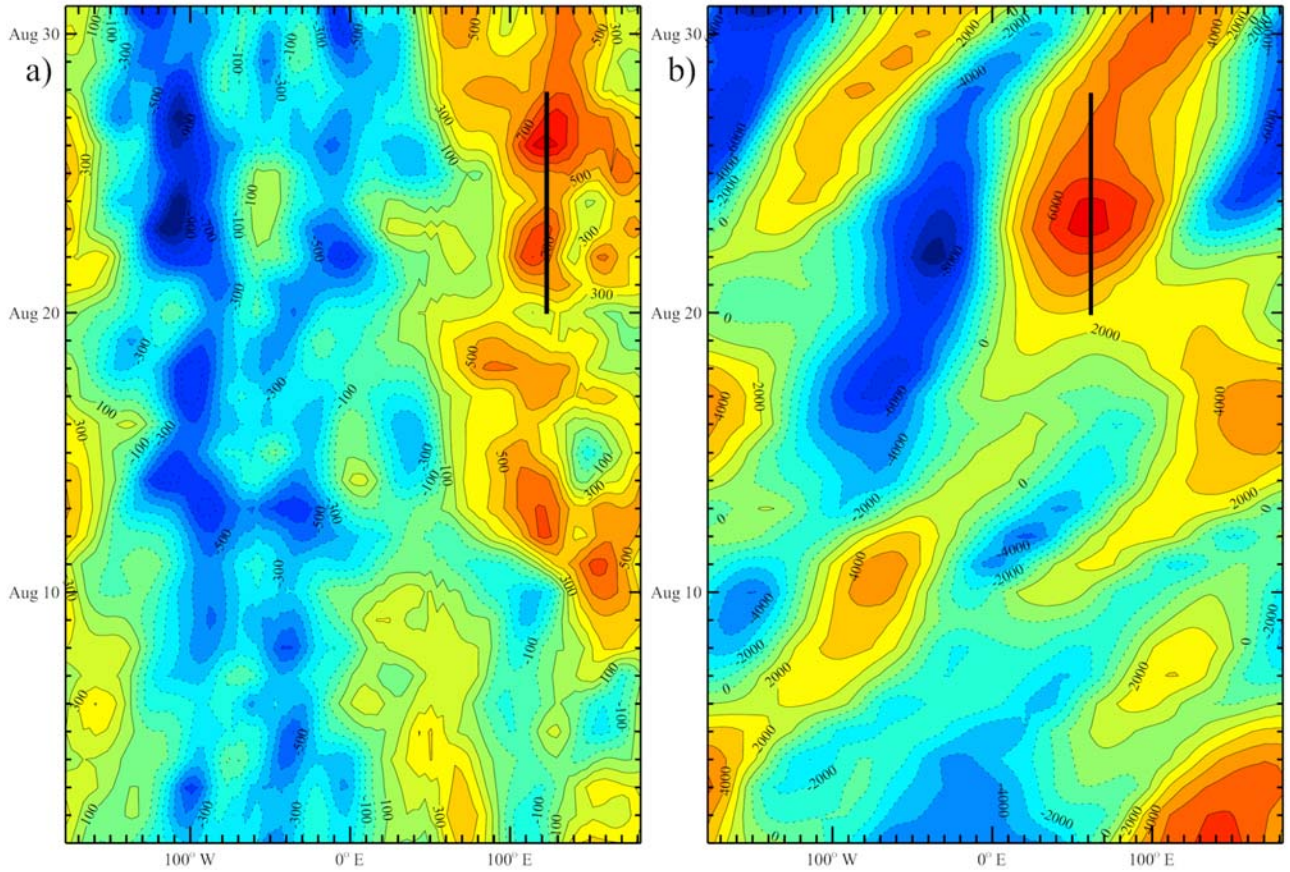

Figure 12. Longitude-time sections of UKMO eddy Montgomery stream function during August 2000 at (a) 16°S, 350 K, contour interval 100 m^2 s^{-2} and (b) 46°S, 700 K, contour interval 1000 m^2 s^{-2}. The black line highlights the period August 20–28 when the subtropical Australian High amplified while the extratropical traveling wave two ridge stalled and amplified in the same longitude band. High (low) eddy Montgomery stream function values are indicated in orange (blue).

zonal wave numbers 1–2, with wave two dominating during August 2000.

[47] There is a general tendency for higher amplitude subtropical anticyclones in the Southeast Asian sector (Figure 12a) to coincide with stalling of traveling planetary waves (Figure 12b) during August 1–5, 8–12, 14–18, and 20–28. During August 20–28 the Australian High amplified repeatedly (solid line in Figure 12a) as the ridge near 80°E stalled and amplified, with M' exceeding 6000 $m^2 s^{-2}$ at 700 K on August 24 (solid line in Figure 12b). This planetary wave two remained stalled for over a week. This repeated phenomenon exhibits qualities of anticyclonic vortex merger, with the axis of the resulting hybrid anomaly extending poleward and westward with altitude.

[48] Many similar sequences exist in the years examined (1990–2004). During 2002, traveling wave two stalled in early and in mid-September [*Harnik et al.*, 2005, Figure 8]. *Lahoz et al.* [2006] discussed flow evolution during southern spring 2003, with notable features including the merger of anticyclones in the stratosphere and the development of an intense, quasi-stationary anticyclone in spring. Between the end of August and the end of October 2003, this quasi-stationary anticyclone gradually grew in strength and moved toward the sector between 90°E and 90°W. This preferred longitude band is a prominent feature of the middle stratosphere in the anticyclone climatology of *Harvey et al.* [2002].

[49] The horizontal and vertical structure of the SIO anticyclone and wave two ridge on 24 August 2000 is shown in Figure 13. The anticyclone over the SIO just west of Australia at 360 K (Figure 13c) tilts westward and poleward with height to 525 K (Figure 13b), consistent with linear Rossby wave theory. The traveling wave two ridge at 525 and 800 K is greatly amplified in this quadrant. The ridge in Figure 13b is accompanied by poleward flow over the South Atlantic, then eastward flow along its poleward side near 47.5°S (arrows in Figure 10b). Lagrangian parcel trajectories (not shown) go around the polar vortex many times as they subside over the course of many days. The downward arrow near Australia in Figure 10b suggests that ozone-rich air coming from the subtropical Atlantic middle stratosphere, after rounding Antarctica many times, may eventually descend into a synoptic wave trough in the upper troposphere just southwest of Australia (Figure 13c).

[50] This suggests an ozone transport pathway out of the tropical Atlantic, where vertical sheets of high ozone air are wrapped around and into the base of a stalled wave 2 ridge

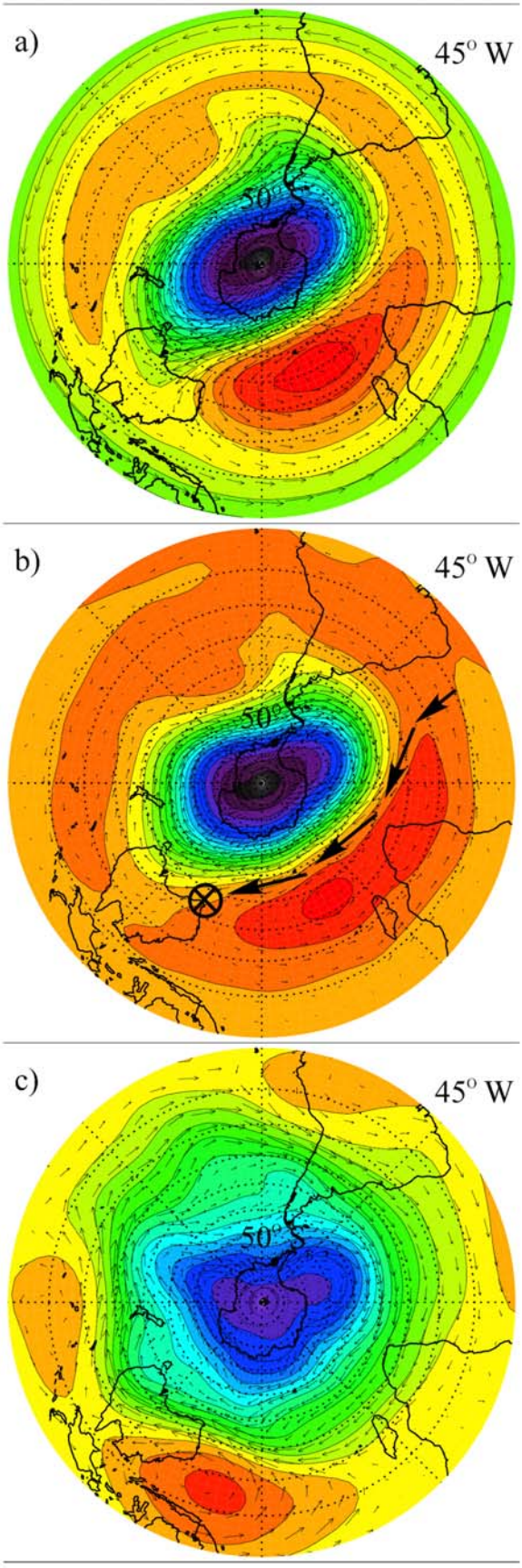

near Australia, with the lower portion descending into synoptic troughs in the UTLS preferentially in this longitude band. Previous studies have found a preferred pathway for ozone and volcanic aerosol out of the tropical stratosphere into the SH in the Atlantic sector [*Leovy et al.*, 1985; *Trepte et al.*, 1993; *Randel et al.*, 1993; *Hitchman et al.*, 1994; *Knox and Harvey*, 2005].

[51] The spatial relationship between ozone and the Aleutian High during the northern winter is very similar, with high ozone within the anticyclone [*Harvey and Hitchman*, 1996]. The source of air for the Aleutian High during boreal winter is also commonly over the tropical Atlantic [*Leovy et al.*, 1985; *Lahoz et al.*, 1994; *Harvey et al.*, 1999]. Extratropical anticyclones have tropical air mass characteristics, with enhanced ozone and small absolute vorticity. The strong correlation between high ozone and anticyclones in the stratosphere is documented by *Harvey et al.* [2004].

[52] A longitude-altitude section of Z' at 22°S on 24 August 2000 is shown in Figure 14. At this latitude the SIO high and wave two ridge appear to be continuous with each other. The amplitude of the upper stratospheric ridge near 0–60°E is much larger than the one near 120–160°W (Figure 14a). In panel b, height anomalies were scaled by $e^{-z/2H}$ to compare Rossby wave activity magnitudes across altitude. A continuous anticyclone is observed, with wave activity diminishing upward and westward from the Australian High. Progressing from the subtropics to the extratropics, the AH gradually blends into the wave two ridge as it grows in eddy height amplitude (Figure 14a).

5. Ten Year Climatological Structure and Momentum Budget

5.1. Wind and Height Anomalies for August and October

[53] The Australian jet near 150 hPa is featured in 10-year averages of ECMWF data for August and October in Figures 15a and 15b. During August the entrance to the Australian subtropical westerly jet is located near 30°S, 70°E and the jet exit region is located near 140°W. The broad tropical easterly flow equatorward of the Tibetan High transitions to westerly flow near 30°S, with $\frac{\partial u}{\partial y} \sim -70$ m/s from 30°S to the equator. This implies that the southward flow into the southern Indian Ocean is inertially unstable from the equator to ~8°S, with weak inertial stability to ~30°S. By October the winter westerlies have weakened and the yellow area for flow exceeding 35 m/s is much smaller, indicating a pronounced zonal contraction and weakening of the jet over Australia (Figure 15b).

Figure 13. ECMWF Montgomery stream function and wind vectors, 1200 UT 24 August 2000 at (a) 800 K, contour interval 4.5×10^7 m^2 s^{-2}, (b) 525 K, contour interval 3×10^7 m^2 s^{-2}, and (c) 360 K, contour interval 4×10^7 m^2 s^{-2}. Arrows in Figure 13b suggest an ozone transport pathway from the subtropical South Atlantic, around the ridge along its poleward side, with a spiral descent at the edge of the polar vortex, eventually into the top of a synoptic trough near Australia in Figure 13c. High (low) Montgomery stream function values are indicated in orange (blue).

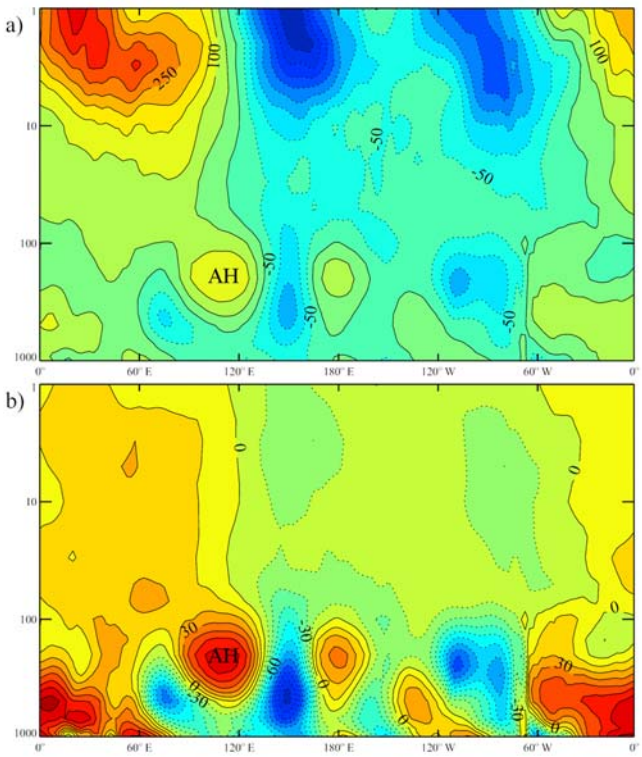

Figure 14. Altitude-longitude section at 22°S of ECMWF (a) eddy geopotential height, Z' contour interval 50 m, and of (b) $Z'\ e^{-z/2H}$, contour interval 10 m, at 1200 UT 24 August 2000. Positive (negative) eddy height perturbations are highlighted in orange (blue).

[54] The corresponding UTLS meridional outflow into the southern Indian Ocean is shown in Figures 15c and 15d. Southward flow near 14 km reaches −9 m/s near Diego Garcia in August (see Figure 4a and *Yao* [1994]). The zero wind line for the meridional wind component lies near 30°S in the western and central SIO. This southward meridional jet ends at the entrance to the westerly Australian jet (compare Figures 15a and 15c and Figures 15b and 15d). The southward meridional flow is weaker in October (Figures 15c and 15d) and the Australian jet is noticeably shorter in longitude than in August (Figures 15a and 15b). This jet contraction is related to the seasonal zonal contraction of convection (Figure 3).

[55] The ten year mean ECMWF distribution of 150 hPa Z' is shown for August and October in Figures 15e and 15f. In daily synoptic maps UTLS anticyclones over the SIO can occur near South Africa, over the SIO, or over Australia. In the August mean a large SIO high is found at the tip of the meridional outflow, south of Madagascar (Figure 15e). Note that this South Indian Ocean High is associated with strengthening of the polar night jet on its poleward periphery (Figures 15a and 15e).

[56] In October distinct South African and Australian Highs are seen (Figure 15f). This seasonal development may be related to strengthening convection over southern Africa and the zonal contraction and eastward migration over Indonesia (Figure 3b). These SIO anticyclones reside at the poleward edge of the monsoon outflow and represent the boundary between subtropical, nearly inertially neutral flow, and midlatitude quasi-geostrophic flow. Note that the Australian High lies just equatorward of the Australian westerly jet entrance in the October monthly mean, while the South African High lies just equatorward of the 35 m/s contour of the polar night jet (Figures 15b and 15f).

5.2. Convective Outflow and the Momentum Budget of the Australian Jet

[57] The zonal momentum equation in log-pressure coordinates on a sphere is

$$\frac{\partial u}{\partial t} + u\frac{\partial u}{\partial x} + v\frac{\partial u}{\partial y} + w\frac{\partial u}{\partial z} - fv + g\frac{\partial Z}{\partial x} = X \qquad (1')$$

where X is the body force due to surface work by nonconservative subgrid-scale processes, including turbulence and wave drag, $dx = a\cos\phi d\lambda$, and $dy = ad\phi$, where a is the earth's radius, λ is longitude and ϕ is latitude [*Andrews et al.*, 1987]. For monthly averages, [ ], (1) may be written

$$\frac{\delta[u]}{\delta t} + \left[u\frac{\partial u}{\partial x}\right] + \left[v\frac{\partial u}{\partial y}\right] + \left[w\frac{\partial u}{\partial z}\right] - f[v] + g\left[\frac{\partial Z}{\partial x}\right] = [X]. \qquad (2)$$

$[X]$ may be estimated as a residual of the terms on the left hand side of (2). $[X]$ is likely to be non-negligible near thunderstorm tops and above mountain ranges. It is difficult to estimate the vertical advection term because of the moderate vertical resolution of global data sets and fundamental uncertainty in vertical velocity fields. Here we use (2) to compare the spatial patterns of jet accelerations with those of meridional advection of angular momentum. Estimates of $[X]$ and $[w\frac{\partial u}{\partial z}]$, which tend to be small, are excluded from this analysis.

[58] The term $[u\frac{\partial u}{\partial x}]$ represents the spatial acceleration (jet entrance) and deceleration (jet exit) of the monthly mean jet. *Lau and Wallace* [1979] and *White* [1982] have shown that subtropical westerly jet entrances are most fundamentally the result of ageostrophic outflow from tropical convection in the approximate balance $[u\frac{\partial u}{\partial x}] \approx f[v_a]$, where $v_a = v - v_g$ and $fv_g = g\frac{\partial Z}{\partial x}$.

[59] Neglecting small-scale body forces and vertical advection, (2) may be written

$$\left[u\frac{\partial u}{\partial x}\right] \approx \left[\left(f - \frac{\partial u}{\partial y}\right)v\right] - g\left[\frac{\partial Z}{\partial x}\right] - \frac{\delta[u]}{\delta t}. \qquad (3)$$

The l.h.s. of (3) may be compared with the first bracketed term on the r.h.s. of (3) to observe the geographical coincidence of meridional advection of angular momentum and spatial acceleration of the jet. The l.h.s. of (3) may be compared with the sum of terms on the r.h.s of (3) to examine the relationship found by *Lau and Wallace* [1979] and *White* [1982]. The seasonal trend in zonal wind is significant and needs to be included to obtain good spatial agreement, thereby validating the assumptions in approximation (3).

[60] Terms in the 10-year zonal momentum budgets at 150 hPa for August on the left and October on the right are shown in Figure 16. From top to bottom, Figure 16 shows zonal spatial acceleration $[u\frac{\partial u}{\partial x}]$ (l.h.s. of (3)), meridional

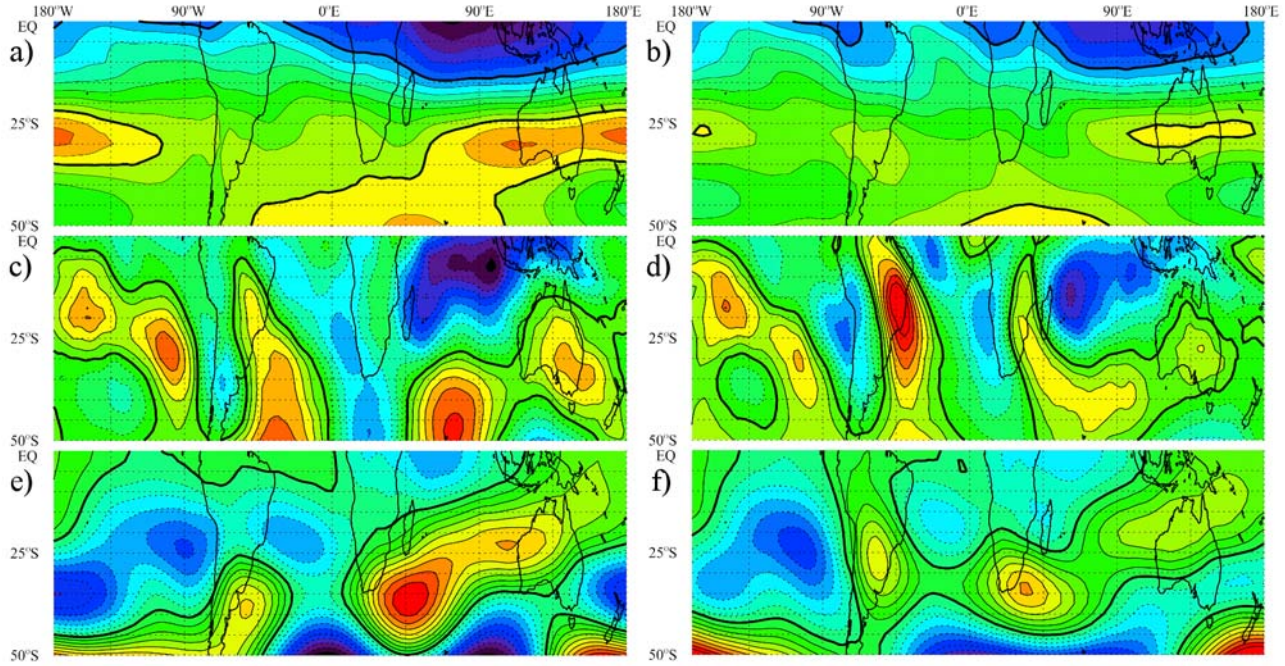

Figure 15. ECMWF 10 year average (1995–2004) 150 hPa (a) August and (b) October zonal wind (−30 to 50 m/s every 5 m/s, with 0 m/s and 35 m/s indicated by heavy black contours and yellow indicating above 35 m/s), (c) August and (d) October meridional wind (−12 to 8 m/s every 1 m/s, with 0 m/s indicated by a heavy black contour), and (e) August and (f) October geopotential height anomaly (−1400 to 1900 m every 100 m, with zero contour highlighted). Note the zonal contraction of the Australian subtropical westerly jet (ASWJ) from August (Figures 15a, 15c, and 15e) to October (Figures 15b, 15d, and 15f) and the splitting of the southern Indian Ocean (SIOH) in this long-term climatology. Note the coincidence of the jet entrance axis with the farthest southward extent of outflow over the Indian Ocean. In each plot, large positive (negative) values are indicated in orange (blue).

advection of angular momentum $[(f - \frac{\partial u}{\partial y})v]$ (first bracketed term on r.h.s. of (3)), and the sum of all terms on the r.h.s. of (3).

[61] Spatial acceleration of the zonal wind exhibits a broad positive region between South Africa and Australia near 30°S in both August and October (Figures 15a, 15b, 16a, and 16b), while a negative region is seen near 25°S in the jet exit region over the Eastern Pacific. Standing orographic gravity waves show up strikingly over the Andes in the ECMWF analyses in the climatological monthly mean spatial acceleration term (Figures 16a and 16b).

[62] Meridional advection of angular momentum is shown in Figures 16c and 16d. Note the general correspondence between the patterns of spatial acceleration and meridional advection of angular momentum over the SIO between Africa and Australia (Figures 16a and 16c and Figures 16b and 16d). There is also reasonable correspondence between deceleration in the jet exit region over the Eastern Pacific and equatorward flow (compare Figures 15c and 16a and 16c; Figures 15d and 16b and 16d). Outflow from Indonesian convection in the UTLS exports a large amount of westerly angular momentum and creates a large region of westerly acceleration in the SIO north of 30°S.

[63] Careful examination reveals that the region of jet acceleration is located near 30°S but the maximum in meridional advection of angular momentum is closer to 15°S. By including the height gradient term and time rate of change of zonal wind (all terms on the r.h.s. of (3)), better agreement is found with the pattern and magnitude of spatial acceleration near the ASWJ entrance and exit (compare Figures 16a and 16e and Figures 16b and 16f). This validates the relationship between ageostrophic advection of angular momentum from tropical convective outflow and subtropical jet entrance location that was found by *Lau and Wallace* [1979] and *White* [1982]. This confirms the fundamental role of tropical convective outflow in creating the SIOH in the subtropics and supplying angular momentum to the Australian westerly jet.

5.3. Planetary Wave Trains in August and October

[64] In order to more completely understand the seasonal strengthening and eastward shift in the ozone maximum it is useful to examine the changes in monthly mean geopotential height anomalies at several levels in the stratosphere (Figure 17). The 10-year climatology for August shows a pair of anticyclones straddling the equatorial Indian Ocean at 100 hPa (Figure 17e) with a planetary wave train emanating into the SH. The SH anticyclone centered near the Date Line exceeds 175 m amplitude at 100 hPa and exceeds 250 m at 50 hPa and 450 m at 10 hPa. Note that the NH summer easterlies (Figures 4a and 7a) prevent propagation of tropical planetary wave energy associated with quasi-stationary monsoon anticyclones at 100 hPa (Figure 17e) to the 50 and

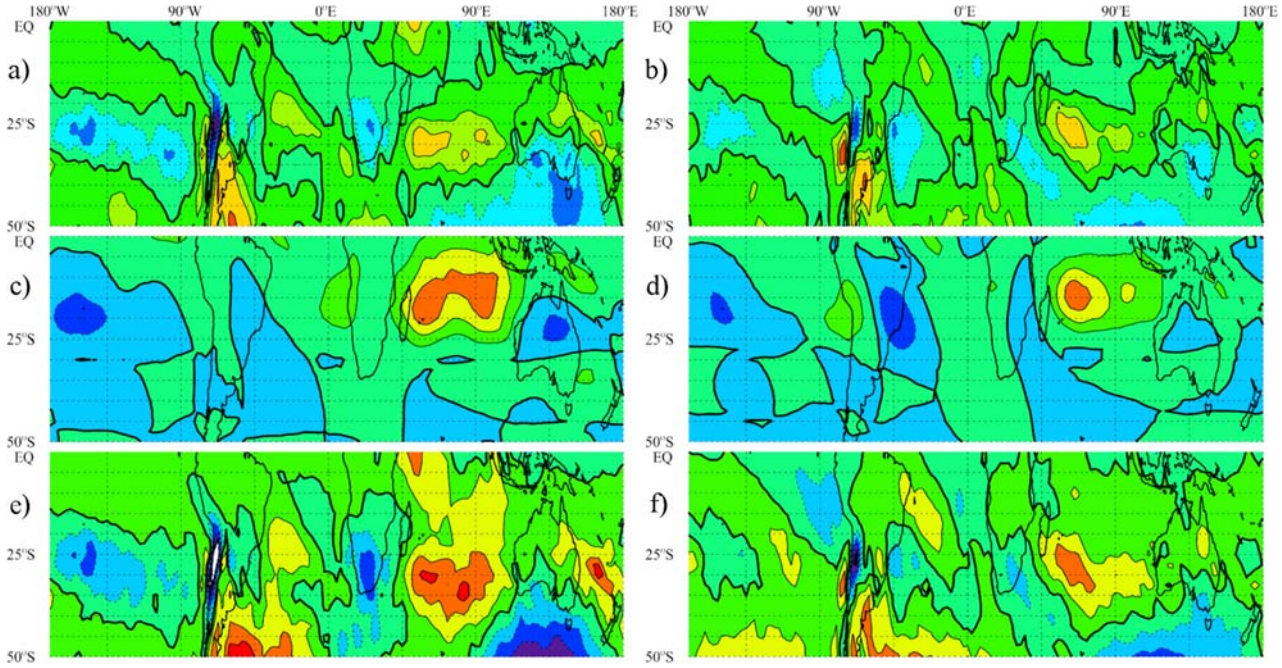

Figure 16. ECMWF 10 year average (1995–2004) terms in the zonal momentum budget at 150 hPa for (a) August and (b) October spatial acceleration of zonal wind, $[u\frac{\partial u}{\partial x}]$, with contours from −1.3 to 1.0 every 0.1, (c) August and (d) October meridional advection of absolute vorticity, $[(f-\frac{\partial u}{\partial y})v]$, with contours from −1.0 to 1.1 every 0.1, and (e) August and (f) October the sum of the terms on the right hand side of (3), with contours from −1.4 to 1.1 every 0.1. Accelerations are given in units of 10^{-3} m s^{-2} (or 100 m s^{-1} day^{-1}). In each plot, large positive (negative) values are indicated in orange (blue) and the zero contour for each quantity is emphasized in heavy black. Note the agreement near 30°S between Figures 16a and 16e and Figures 16b and 16f in the pattern and magnitude in the ASWJ entrance region over the SIO and the exit region over the Eastern Pacific.

10 hPa levels (Figures 17a and 17c), in accordance with the Charney-Drazin criterion [*Andrews et al.*, 1987]:

$$0 < \overline{u} - c < \frac{\beta}{K^2},$$

where $K^2 = k^2 + l^2 + (f^2/N^2)m^2$. For quasi-stationary subtropical UTLS anticyclones $c \approx 0$, so $\overline{u} > 0$ is required for transmission of planetary Rossby wave energy into the extratropical stratosphere.

[65] During October convection shifts eastward (Figure 3), as does the Tibetan High in the UTLS (Figures 17e and 17f). The SIOH has a center near South Africa and one near Australia (Figures 15e and 15f and Figures 17e and 17f), the latter being consistent with an eastward shift of Indonesian convection. The SH midlatitude anticyclone near the Date Line exceeds 250 m amplitude at 100 hPa (Figure 17f), an increase of ~40% over August (Figure 17e). This agrees with the positions of the stalled ridges observed by *Mechoso et al.* [1988] and highlights the relevance of their work to the ozone maximum. The midlatitude ridge maximum occurs precisely where the ozone maximum grows from August to October (Figure 1 and auxiliary material Figure S1). This structure in October is more effective at transporting ozone out of the sunlit tropics into the poleward side and base of the ridge (see Figures 10b and 13b), ultimately becoming available for convergence into a synoptic wave trough (Figures 10b and 13c).

[66] Note that in October westerly winds in the NH allow planetary Rossby waves to radiate into the extratropical stratosphere from Indonesian convection (Figures 17b, 17d, and 17f). Convectively-driven subtropical anticyclones in the UTLS and the resultant radiation of a planetary wave pattern constitute a direct tropical forcing mechanism for influencing the general circulation of the extratropical stratosphere whenever there are westerly winds connecting the two regions.

6. Conclusions

[67] During austral winter and spring monthly mean column ozone near 40–60°S exhibits a zonally asymmetric maximum centered near Australia, which extends from the southern Indian Ocean to the Eastern Pacific and amplifies from August to October. We propose that this ozone anomaly results from deep convective outflow over Southeast Asia and Indonesia, which drives a broad southwestward current in the upper troposphere and lower stratosphere across the equator far into the SIO. The effects may be categorized into three primary dynamical processes: (1) Tropical convective outflow from Indonesia controls the location of the subtropical anticyclones and position of the Australian Subtropical Westerly Jet. (2) Synoptic Rossby waves breaking

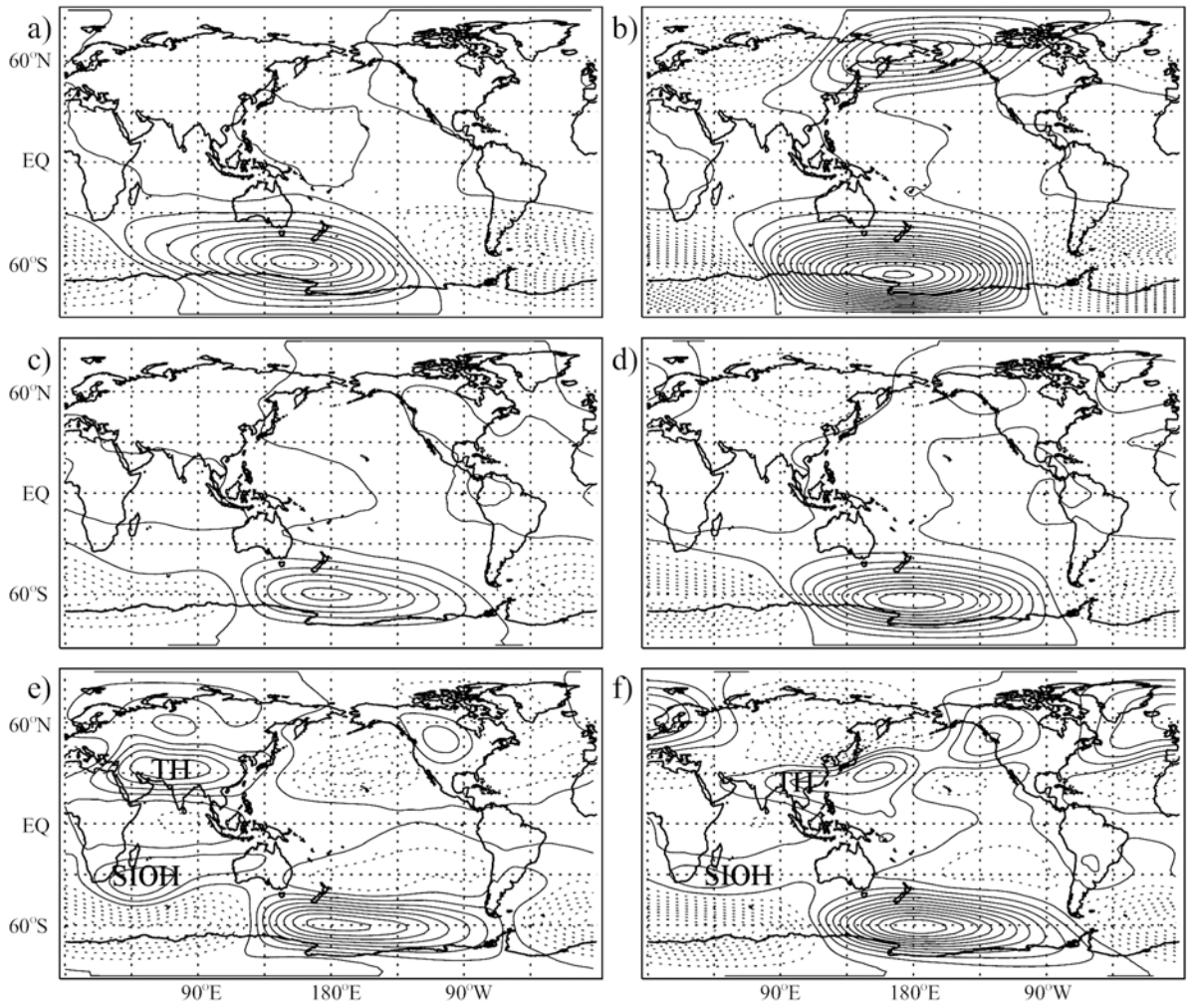

Figure 17. ECMWF 10 year average (1995–2004) monthly mean eddy geopotential height anomalies, Z', for (a) August and (b) October at 10 hPa, contour interval 50 m, (c) August and (d) October at 50 hPa, contour interval 50 m, and (e) August and (f) October at 100 hPa, contour interval 25 m. Positive (negative) height anomalies are indicated with solid (dashed) contours. Note that very little Rossby wave activity radiates upward from the Tibetan High (TH) into the summer easterlies while a clear planetary wave train emanates from the southern Indian Ocean high (SIOH) into winter westerlies and is manifested as a wave one pattern in the extratropical upper stratosphere.

on this jet transport ozone into the ozone maximum on its poleward flank. (3) Subtropical UTLS anticyclones in the SIO sector merge with stalling, amplifying extratropical ozone-rich ridges.

[68] The seasonal change in solar forcing leads to an eastward shift in tropical convection and an eastward shift and intensification of the ozone maximum. Zonal contraction of the convective outflow leads to a zonally contracted ASWJ, which contributes to the amplification of the OM through locally-enhanced ozone transport by synoptic waves. More importantly, an Australian High amplifies from August through October, which interacts with traveling planetary wave two ridges, which become more prevalent in the SH as winter westerlies relax. A significant enhancement of the ozone maximum occurs through frequent stalling of traveling planetary wave ridges, which merge with the Australian High.

[69] An interhemispheric transport pathway from the northern lower stratosphere to the southern lower stratosphere is identified, which travels around the Tibetan High, across the equator, and around the SIO High. It crosses thousands of km of frequent deep convection, where detrainment overwhelmingly dilutes the air in this current with tropical tropospheric air. The nearly inertially neutral southward flow into the SIO helps to create an adverse height gradient, the southwest-northeast tilting SIO High. This is to be contrasted with the ozone transport pathway into the OM. The role of planetary wave ridges in transporting ozone from the tropics poleward and downward into the lower stratosphere is highlighted, with ultimate entry into synoptic wave troughs in the region of the OM.

[70] The primary changes in column ozone from August to October amount to an eastward rotation and amplification of the wave one ozone maximum/ozone hole pattern (Figure 1).

This is consistent with the eastward shift in convection and amplification of the Australian High/planetary wave pattern.

[71] This connection between the geographical distribution of ozone and Asian monsoon outflow illustrates that Asian summer monsoon variability can directly affect the major features of the ozone distribution in the Southern Hemisphere. This study supports the concept that Rossby wave activity associated with subtropical monsoon anticyclones can propagate through westerlies and influence the extratropical stratosphere. The southern Indian Ocean region seems to be a particularly sensitive region for the transmission of wave activity from the tropics to the SH extratropical stratosphere.

[72] **Acknowledgments.** We thank Adrian Tuck, Steve Pawson, Walter Robinson, and Greg Postel for useful conversations, Amihan Huesmann for creating the RWB statistics, and Ivanka Stajner and Hiroo Hayashi for providing the GMAO data available from the year 2000. This work was supported by funding from the National Science Foundation and the National Aeronautics and Space Administration.

References

Andrews, D. G., J. R. Holton, and C. B. Leovy (1987), *Middle Atmosphere Dynamics*, 498 pp., Academic, San Diego, Calif.

Annamalai, H., J. M. Slingo, K. R. Sperber, and K. Hodges (1999), The mean evolution and variability of the Asian summer monsoon: Comparison of ECMWF and NCEP-NCAR reanalyses, *Mon. Weather Rev.*, *127*, 1157–1186.

Aoki, H., M. Shiotani, and I. Hirota (1996), Interannual variability of the tropospheric circulation and its relation to the stratosphere in the Southern Hemisphere, *J. Meteorol. Soc. Jpn.*, *74*, 509–523.

Berberry, E. H., J. Nogues-Paegle, and J. D. Horel (1992), Wavelike Southern Hemisphere extratropical teleconnections, *J. Atmos. Sci.*, *49*, 155–177.

Bjerknes, V., J. Bjerknes, T. Bergeron, and H. Solberg (1933), *Physikalische Hydrodynamik*, 797 pp., Springer, New York.

Butchart, N., et al. (2006), Simulations of anthropogenic change in the strength of the Brewer-Dobson circulation, *Clim. Dyn.*, *27*, 727–741.

Charlton, A. J., A. O'Neill, W. A. LaHoz, and P. Berrisford (2005), The splitting of the stratospheric polar vortex in the Southern Hemisphere, September 2002: Dynamical evolution, *J. Atmos. Sci.*, *62*, 590–602.

Crook, J. A., N. P. Gillet, and S. Keeley (2008), Sensitivity of Southern Hemisphere climate to zonal asymmetry in ozone, *Geophys. Res. Lett.*, *35*, L07806, doi:10.1029/2007GL032698.

Dickinson, R. E. (1971), Cross-equatorial eddy momentum fluxes as evidence of tropical planetary wave sources, *Q. J. R. Meteorol. Soc.*, *97*, 554–558.

Eyring, V., et al. (2006), Assessment of temperature, trace species, and ozone in chemistry climate model simulations of the recent past, *J. Geophys. Res.*, *111*, D22308, doi:10.1029/2006JD007327.

Garcia, R. R., and W. J. Randel (2008), Acceleration of the Brewer-Dobson circulation due to increases in greenhouse gases, *J. Atmos. Sci.*, *65*, 2731–2739.

Gill, A. E. (1980), Some simple solutions for heat-induced tropical circulation, *Q. J. R. Meteorol. Soc.*, *106*, 447–462.

Gillet, N. P., and D. Thompson (2003), Simulation of recent Southern Hemisphere climate change, *Science*, *302*, 273–275.

Godson, W. L. (1963), in *Meteorological Abhandlungen*, vol. 35, pp. 161–206, Free Univ. of Berlin Press, Berlin.

Grytsai, A. V., et al. (2007), Structure and long-term change in the zonal asymmetry in Antarctic total ozone during spring, *Ann. Geophys.*, *25*, 361–374.

Harnik, N., R. K. Scott, and J. Perlwitz (2005), Wave reflection and focusing prior to the major stratospheric warming of September 2002, *J. Atmos. Sci.*, *62*, 640–650.

Hartmann, D. L. (1977), Stationary planetary waves in the Southern Hemisphere, *J. Geophys. Res.*, *82*, 4930–4934.

Harvey, V. L., and M. H. Hitchman (1996), A climatology of the Aleutian High, *J. Atmos. Sci.*, *53*, 2088–2101.

Harvey, V. L., M. H. Hitchman, R. B. Pierce, and T. D. Fairlie (1999), Tropical high aerosol in the Aleutian anticyclone, *J. Geophys. Res.*, *104*, 6281–6290.

Harvey, V. L., R. B. Pierce, T. D. Fairlie, and M. H. Hitchman (2002), A climatology of stratospheric polar vortices and anticyclones, *J. Geophys. Res.*, *107*(D20), 4442, doi:10.1029/2001JD001471.

Harvey, V. L., R. B. Pierce, M. H. Hitchman, C. E. Randall, and T. D. Fairlie (2004), On the distribution of ozone in stratospheric anticyclones, *J. Geophys. Res.*, *109*, D24308, doi:10.1029/2004JD004992.

Haynes, P. H., C. J. Marks, M. E. McIntyre, T. G. Shepherd, and K. P. Shine (1991), On the "downward control" of extratropical diabatic circulations by eddy-induced mean zonal forces, *J. Atmos. Sci.*, *48*, 651–678.

Hendon, H. H., and D. L. Hartmann (1982), Stationary waves on a sphere: Sensitivity to thermal feedback, *J. Atmos. Sci.*, *39*, 1906–1920.

Hio, Y., and S. Yoden (2005), Interannual variations of the seasonal march in the Southern Hemisphere stratosphere for 1979–2002 and characterization of the unprecedented year 2002, *J. Atmos. Sci.*, *62*, 567–580.

Hio, Y., and S. Yoden (2007), A parameter sweep experiment on quasi-periodic variations of a polar vortex due to wave-wave interaction in a spherical barotropic model, *J. Atmos. Sci.*, *64*, 4069–4083.

Hitchman, M. H., and A. S. Huesmann (2007), A climatology of Rossby wave breaking: Seasonal distributions and dynamical regimes, *J. Atmos. Sci.*, *64*, 1922–1940.

Hitchman, M. H., and A. S. Huesmann (2009), Effect of the Quasibiennial Oscillation on stratospheric jets and Rossby wave breaking, *J. Atmos. Sci.*, *66*, 935–946.

Hitchman, M. H., and M. J. Rogal (2010), ENSO influences on monthly mean column ozone and stratospheric geopotential height and temperature anomalies during the Southern Hemisphere winter to spring transition, *J. Geophys. Res.*, doi:10.1029/2009JD012844, in press.

Hitchman, M. H., M. McKay, and C. R. Trepte (1994), A climatology of stratospheric aerosol, *J. Geophys. Res.*, *99*, 20,689–20,700.

Hollingsworth, A., et al. (1986), Monitoring of observation and analysis quality by a data assimilation system, *Mon. Weather Rev.*, *114*, 861–879.

Hudson, R. D., A. D. Frolov, M. F. Andrade, and M. B. Follette (2003), The total ozone field separated into meteorological regimes. Part I: Defining the regimes, *J. Atmos. Sci.*, *60*, 1669–1677.

Hurrell, J. W., H. van Loon, and D. J. Shea (1998), The mean state of the troposphere, in *Meteorology of the Southern Hemisphere*, pp. 1–46, Am. Meteorol. Soc., Boston, Mass.

Johnson, D. R. (1989), The forcing and maintenance of global monsoon circulations: An isentropic analysis, *Adv. Geophys.*, *31*, 43–316.

Kallberg, P., et al. (2005), ERA-40 atlas, *Re-Anal. Project Rep. Ser. 19*, 191 pp., ECMWF, Reading, U. K.

Kalnay, E., et al. (1996), The NCEP/NCAR 40-Year Reanalysis Project, *Bull. Am. Meteorol. Soc.*, *77*, 437–471.

Keyser, D., and M. A. Shapiro (1986), A review of the structure and dynamics of upper-level frontal zones, *Mon. Weather Rev.*, *114*, 452–499.

Kida, H. (1977), A numerical investigation of the atmospheric general circulation and stratospheric-tropospheric mass exchange: II. Lagrangian motion of the atmosphere, *J. Meteorol. Soc. Jpn.*, *55*, 71–88.

Kiladis, G. N., and K. C. Mo (1998), Interannual and intraseasonal variability in the Southern Hemisphere, in *Meteorology of the Southern Hemisphere*, pp. 307–336, Am. Meteorol. Soc., Boston, Mass.

Knox, J. A., and V. L. Harvey (2005), Global climatology of inertial instability and Rossby wave breaking in the stratosphere, *J. Geophys. Res.*, *110*, D06108, doi:10.1029/2004JD005068.

Krishnamurti, T. N., S. M. Daggiupaty, J. Fein, M. Kanamitsu, and J. D. Lee (1973), Tibetan High and upper tropospheric tropical circulations during northern summer, *Bull. Am. Meterol. Soc.*, *54*, 1234–1249.

Lahoz, W. A., et al. (1994), Three dimensional evolution of water vapour distributions in the Northern Hemisphere stratosphere as observed by the Microwave Limb Sounder, *J. Atmos. Sci.*, *51*, 2914–2930.

Lahoz, W. A., A. J. Geer, and A. O'Neill (2006), Dynamical evolution of the 2003 Southern Hemisphere stratospheric winter using Envisat trace-gas observations, *Q. J. R. Meteorol. Soc.*, *132*, 1985–2008.

Lau, N.-C., and J. M. Wallace (1979), On the distribution of horizontal transports by transient eddies in the Northern Hemisphere wintertime circulation, *J. Atmos. Sci.*, *36*, 1844–1861.

Leovy, C. B., and P. J. Webster (1976), Stratospheric long waves: Thermal structure in the Northern and Southern Hemispheres, *J. Atmos. Sci.*, *33*, 1624–1638.

Leovy, C. B., et al. (1985), Transport of ozone in the middle stratosphere: Evidence for planetary wave breaking, *J. Atmos. Sci.*, *42*, 230–244.

Liebmann, B., and D. L. Hartmann (1982), Interannual variations of outgoing IR associated with tropical circulation changes, *J. Atmos. Sci.*, *39*, 1153–1162.

London, J., R. D. Bojkov, S. Oltmans, and J. I. Kelley (1976), Atlas of the global distribution of total ozone, July 1957–June 1967, *NCAR Tech. Note 113*, 276 pp., Natl. Cent. for Atmos. Res., Boulder, Colo.

MacDowall, J. (1960), Some observations at Halley Bay in seismology, glaciology, and meteorology, *Proc. R. Soc. A*, *256*, 149–196.

Mechoso, C. R., and D. L. Hartmann (1982), An observational study of traveling planetary waves in the Southern Hemisphere, *J. Atmos. Sci.*, *39*, 1921–1935.

Mechoso, C. R., A. O. Neill, V. D. Pope, and J. D. Farrara (1988), A study of the stratospheric final warming of 1982 in the Southern Hemisphere, *Q. J. R. Meteorol. Soc.*, *114*, 1365–1384.

Nathan, T. R., and E. C. Cordero (2007), An ozone-modified refractive index for vertically propagating planetary waves, *J. Geophys. Res.*, *112*, D02105, doi:10.1029/2006JD007357.

Newell, R. E., J. W. Kidson, D. G. Vincent, and G. J. Boer (1972), *The General Circulation of the Tropical Atmosphere and Interactions With Extratropical Latitudes*, vol. 2, 371 pp., MIT Press, Cambridge, Mass.

Newman, P. A., and E. R. Nash (2005), The unusual Southern Hemisphere stratosphere winter of 2002, *J. Atmos. Sci.*, *62*, 614–628.

Newman, P. A., and W. J. Randel (1988), Coherent ozone-dynamical changes during the Southern Hemisphere spring, *J. Geophys. Res.*, *93*, 12,585–12,606.

Nogues-Paegle, J. E., and K. C. Mo (1988), Transient response of the Southern Hemisphere subtropical jet to tropical forcing, *J. Atmos. Sci.*, *45*, 1493–1530.

Nogues-Paegle, J. E., and Z. Zhen (1987), The Australian subtropical jet during the second observing period of the Global Weather Experiment, *J. Atmos. Sci.*, *44*, 2277–2289.

Olsen, M. A., M. R. Schoeberl, and A. R. Douglass (2004), Stratosphere-troposphere exchange of mass and ozone, *J. Geophys. Res.*, *109*, D24114, doi:10.1029/2004JD005186.

O'Sullivan, D. J., and T. J. Dunkerton (1995), Generation of inertia-gravity waves in a simulated lifecycle of baroclinic instability, *J. Atmos. Sci.*, *52*, 3695–3716.

Pierce, R. B., and T. D. A. Fairlie (1993), Chaotic advection in the stratosphere: Implications for the dispersal of chemically perturbed air from the polar vortex, *J. Geophys. Res.*, *98*, 18,589–18,595.

Polvani, L. M., and P. J. Kushner (2002), Tropospheric response to stratospheric perturbations in a relatively simple general circulation model, *Geophys. Res. Lett.*, *29*(7), 1114, doi:10.1029/2001GL014284.

Postel, G. A., and M. H. Hitchman (1999), Climatology of Rossby wave breaking along the subtropical tropopause, *J. Atmos. Sci.*, *56*, 359–373.

Quintanar, A. I., and C. R. Mechoso (1995a), Quasi-stationary waves in the Southern Hemisphere. Part I: Observational data, *J. Clim.*, *8*, 2659–2672.

Quintanar, A. I., and C. R. Mechoso (1995b), Quasi-stationary waves in the Southern Hemisphere. Part II: Generation mechanisms, *J. Clim.*, *8*, 2673–2690.

Randel, W. J. (1987), A study of planetary waves in the southern winter troposphere and stratosphere. Part I: Wave structure and vertical propagation, *J. Atmos. Sci.*, *44*, 917–935.

Randel, W. J., and M. Park (2006), Deep convective influence on the Asian summer monsoon anticyclone and associated tracer variability observed with AIRS, *J. Geophys. Res.*, *111*, D12314, doi:10.1029/2005JD006490.

Randel, W. J., and F. Wu (1999), Cooling of the Arctic and Antarctic polar stratospheres due to ozone depletion, *J. Clim.*, *12*, 1467–1479.

Randel, W. J., D. E. Stevens, and J. L. Stanford (1987), A study of planetary waves in the southern winter troposphere and stratosphere. Part II: Life cycles, *J. Atmos. Sci.*, *44*, 936–949.

Randel, W. J., et al. (1993), Stratospheric transport from the tropics to middle latitudes by planetary wave mixing, *Nature*, *365*, 533–535.

Renwick, J. A., and M. J. Revell (1999), Blocking over the South Pacific and Rossby wave Propagation, *Mon. Weather Rev.*, *127*, 2233–2247.

Rodwell, M. J., and B. J. Hoskins (2001), Subtropical anticyclones and summer monsoons, *J. Clim*, *14*, 3192–3211.

Rogal, M. J., M. H. Hitchman, M. L. Buker, G. J. Tripoli, I. Stajner, and H. Hayashi (2010), Modeling the effects of Southeast Asian monsoon outflow on subtropical anticyclones and midlatitude ozone over the southern Indian Ocean, *J. Geophys. Res.*, doi:10.1029/2009JD012979, in press.

Sardeshmukh, P. D., and B. J. Hoskins (1988), The generation of global rotational flow by steady idealized tropical divergence, *J. Atmos. Sci.*, *45*, 1228–1251.

Sato, K., Y. Tomikawa, G. Hashida, T. Yamanouchi, H. Nakajima, and T. Sugita (2009), Longitudinally dependent ozone increase in the antarctic polar vortex revealed by balloon and satellite observations, *J. Atmos. Sci.*, *66*, 1807–1820.

Schneider, E. K., and R. S. Lindzen (1980), Comments on cumulus friction: Estimated influence on the tropical mean meridional circulation, *J. Atmos. Sci.*, *37*, 2803–2806.

Shapiro, M. (1980), Turbulent mixing within tropopause folds as a mechanism for the exchange of chemical constituents between the stratosphere and troposphere, *J. Atmos. Sci.*, *37*, 994–1004.

Shiotani, M., and I. Hirota (1992), Planetary wave-mean flow interaction in the stratosphere: a comparison between Northern and Southern Hemispheres, *Q. J. R. Meteorol. Soc.*, *111*, 309–334.

Shiotani, M., N. Shimoda, and I. Hirota (1993), Interannual variability of the stratospheric ciculation in the Southern Hemisphere, *Q. J. R. Meteorol. Soc.*, *119*, 531–546.

Solomon, S., W. Portmann, T. Sasaki, D. J. Hofmann, and D. W. J. Thompson (2005), Four decades of ozonesonde measurements over Antarctica, *J. Geophys. Res.*, *110*, D21311, doi:10.1029/2005JD005917.

Stajner, I. L., L. P. Riishojgaard, and R. J. Rood (2001), The GEOS ozone data assimilation system: Specification of error statistics, *Q. J. R. Meteorol. Soc.*, *127*, 1069–1094.

Stajner, I., N. Winslow, R. B. Rood, and S. Pawson (2004), Monitoring of observation errors in the assimilation of satellite ozone data, *J. Geophys. Res.*, *109*, D06309, doi:10.1029/2003JD004118.

Stajner, I., K. Wargan, L.-P. Chang, H. Hayashi, S. Pawson, and H. Nakajima (2006), Assimilation of ozone profiles from the Improved Limb Atmospheric Spectrometer-II: Study of Antarctic Ozone, *J. Geophys. Res.*, *111*, D11S14, doi:10.1029/2005JD006448.

Swinbank, R., and A. O'Neill (1994), A stratosphere-troposphere data assimilation system, *Mon. Weather Rev.*, *122*, 686–702.

Thompson, D. W. J., M. P. Baldwin, and S. Solomon (2005), Stratosphere-troposphere coupling in the Southern Hemisphere, *J. Atmos. Sci.*, *62*, 708–715.

Trepte, C. R., R. E. Veiga, and M. P. McCormick (1993), Poleward dispersal of Mt. Pinabuto aerosols, *J. Geophys. Res.*, *98*, 18,563–18,573.

van Loon, H. V., and R. Jenne (1972), The zonal harmonic standing waves in the Southern Hemisphere, *J. Geophys. Res.*, *77*, 992–1003.

Vincent, D. G., and P. L. Silva Dias (1998), Meteorology of the tropics: Pacific Ocean, in *Meteorology of the Southern Hemisphere*, pp. 101–118, Am. Meteorol. Soc., Boston, Mass.

Wallace, J. M. (1978), Trajectory slopes, countergradient heat fluxes and mixing by lower stratospheric waves, *J. Atmos. Sci.*, *35*, 554–558.

White, G. H. (1982), An observational study of the Northern Hemisphere extratropical summertime general circulation, *J. Atmos. Sci.*, *39*, 24–40.

Wirth, V. (1991), What causes the seasonal cycle of stationary planetary waves in the southern stratosphere?, *J. Atmos. Sci.*, *48*, 1194–1200.

Wirth, V. (1993), Quasi-stationary planetary waves in total ozone and their correlation with lower stratospheric temperature, *J. Geophys. Res.*, *98*, 8873–8882.

Yao, C.-Y. (1994), Geographical variation in the annual and quasi-biennial cycles in the tropical lower stratosphere, M. S. thesis, 130 pp., Univ. of Wis.-Madison, Madison.

M. H. Hitchman and M. J. Rogal, Department of Atmospheric and Oceanic Sciences, University of Wisconsin-Madison, 1225 W. Dayton St., Madison, WI 53706, USA. (matt@aos.wisc.edu)